Geological Sciences Faculty Scholarship   College of the Sciences

1-12-2021

Seismicity and Pn Velocity Structure of Central West Antarctica

Erica M. Lucas
Pennsylvania State University

Andrew A. Nyblade
Pennsylvania State University

Andrew J. Lloyd
Washington University in St. Louis

Richard C. Aster
Colorado State University - Fort Collins

Douglas A. Wiens
Washington University in St. Louis

See next page for additional authors

Recommended Citation

Authors

Erica M. Lucas, Andrew A. Nyblade, Andrew J. Lloyd, Richard C. Aster, Douglas A. Wiens, John Paul O'Donnell, Graham W. Stuart, Terry J. Wilson, Ian W. D. Dalziel, J. Paul Winberry, and Audrey D. Huerta

Seismicity and Pn Velocity Structure of Central West Antarctica

Erica M. Lucas[1], Andrew A. Nyblade[1], Andrew J. Lloyd[2], Richard C. Aster[3], Douglas A. Wiens[2], John Paul O'Donnell[4], Graham W. Stuart[4], Terry J. Wilson[5], Ian W. D. Dalziel[6], J. Paul Winberry[7], and Audrey D. Huerta[7]

[1]Department of Geosciences, Pennsylvania State University, PA, USA, [2]Department of Earth and Planetary Sciences, Washington University, St. Louis, MO, USA, [3]Department of Geosciences, Warner College of Natural Resources, Colorado State University, Fort Collins, CO, USA, [4]School of Earth and Environment, University of Leeds, Leeds, WY, UK, [5]School of Earth Sciences, Ohio State University, Columbus, OH, USA, [6]Jackson School of Geosciences, University of Texas at Austin, Austin, TX, USA, [7]Department of Geological Sciences, Central Washington University, Ellensburg, WA, USA

Abstract We have located 117 previously undetected seismic events mainly occurring between 2015 and 2017 that originated from glacial, tectonic, and volcanic processes in central West Antarctica using data recorded on Polar Earth Observing Network (POLENET/ANET) and UK Antarctic Network (UKANET) seismic stations. The seismic events, with local magnitudes (M_L) ranging from 1.1 to 3.5, are predominantly clustered in four geographic regions; the Ellsworth Mountains, Thwaites Glacier, Pine Island Glacier, and Mount Takahe. Eighteen of the events are in the Ellsworth Mountains and can be attributed to a mixture of glacial and tectonic processes. The largest event noted in this study was a mid-crustal (~19 km focal depth; M_L 3.5) normal mechanism earthquake beneath Thwaites Glacier. We also located 91 glacial events near the grounding zones of Thwaites Glacier and Pine Island Glacier that are predominantly associated with time periods of significant calving activity. Eight events, likely arising from volcano-tectonic processes, occurred beneath Mount Takahe. Using Pn travel times from the seismic events, we find laterally variable uppermost mantle structure in central West Antarctica. On average, the Ellsworth Mountains are underlain by a faster mantle lid (V_{Pn} = ~8.4 km/s) compared to the Amundsen Sea Embayment region (V_{Pn} = ~8.1 km/s). Within the Amundsen Sea Embayment itself, we find mantle lid velocities ranging from ~8.05 to 8.18 km/s. Laterally heterogeneous uppermost mantle structure, indicative of variable thermal and rheological structure, likely influences both geothermal heat flux and glacial isostatic adjustment spatial patterns and rates within central West Antarctica.

Plain Language Summary In this study, we have identified and located 117 seismic events in central West Antarctica. The seismic events originate from both solid-Earth and glacial processes. While the seismic events originating from solid-Earth processes are associated with tectonic and volcano-tectonic activity in central West Antarctica, the seismic events arising from glacial processes are predominantly associated with time periods of significant calving activity at Thwaites Glacier and Pine Island Glacier. Using select P-waves produced by seismic events located in this study, we investigate the uppermost portion of the mantle beneath central West Antarctica and find that the temperature of the uppermost mantle likely varies by at least 160 K across central West Antarctica. Variable uppermost mantle temperatures have numerous implications for the dynamics and evolution of the West Antarctic Ice Sheet.

1. Introduction

Although initial studies of Antarctic seismicity were severely limited by the near-absence of seismographs on the continent (e.g., Lander, 1959; Okal, 1981), seismicity patterns associated with a variety of solid Earth and glaciological processes (e.g., Aster & Winberry, 2017) are emerging through ongoing analyses of data collected by several temporary seismic networks during the past 2 decades (e.g., Lough, 2014; Lough et al., 2013, 2018; Olinger et al., 2019; Reading et al., 2007; Smith, 2006; Winberry & Anandakrishnan, 2003; Winberry et al., 2020). In this paper, we provide new observations of Antarctic seismicity by analyzing data collected by recent temporary broadband seismic deployments in central West Antarctica (WANT). We report information on 117 previously undetected seismic events ($1.1 \le M_L \le 3.5$) of glacial, tectonic, and
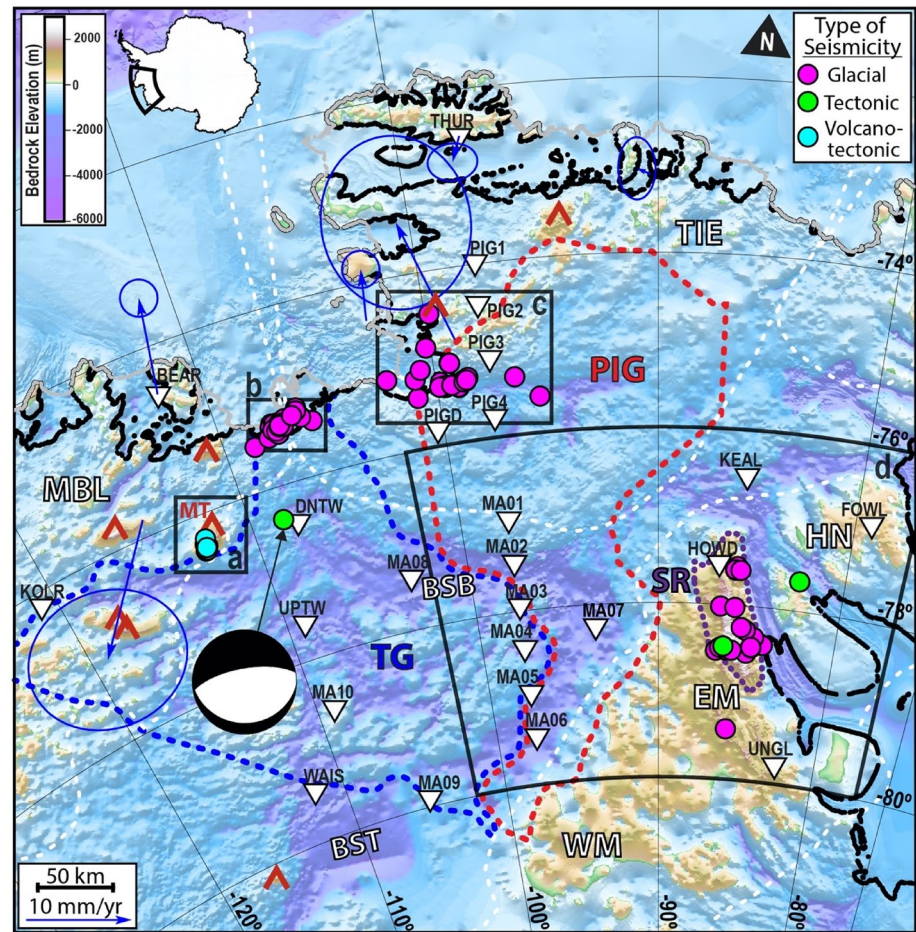
Figure 1. Bedrock topography map of the study area (inset; Morlighem et al., 2020). The grounding line and ice front position are delineated by black and gray lines, respectively (Morlighem et al., 2020). Inverted white triangles mark the locations of seismic stations. Dashed white lines delineate major crustal blocks described in the text; MBL: Marie Byrd Land, TIE: Thurston Island-Eights Coast, and the Haag-Ellsworth Whitmore Mountains. The Thwaites Glacier (TG) and Pine Island Glacier (PIG) catchments are outlined in blue and red dashed lines, respectively. The Sentinel Range (SR) is outlined in a purple dashed line. The partially open dark red triangles mark the locations of subaerial Cenozoic volcanoes (LeMasurier & Thomson, 1990). Blue arrows plot observed horizontal GPS bedrock motions in a frame that fixes East Antarctica (Barletta et al., 2018). Other abbreviated geographic features: EM: Ellsworth Mountains, HN: Haag Nunataks, WM: Whitmore Mountains, MT: Mount Takahe, BST: Bentley Subglacial Trench, BSB: Byrd Subglacial Basin. The gray boxes labeled a, b, c, and d correspond to the locations of the maps in supporting information S7, Figures 2, 7a, and 8a, respectively. The focal mechanism corresponds to the source of the M_L 3.5 Thwaites Glacier earthquake.

volcano-tectonic origin in central WANT, primarily occurring between January 2015 and December 2017 (Figure 1), and use P-wave travel times from these events to constrain uppermost mantle (Pn) velocities.

In this study, we use data from the Polar Earth Observing Network (POLENET/ANET) and UK Antarctic Network (UKANET), which include the first seismographs deployed in WANT that provide sufficient station coverage to study regional seismicity and wave propagation across the Amundsen Sea Embayment and Haag-Ellsworth-Whitmore Mountains regions. The Amundsen Sea Embayment region encompasses the sector of central West Antarctica where Thwaites and Pine Island glaciers flow into the ocean, and the Haag-Ellsworth-Whitmore Mountains region is located upstream of several glaciers, including the Rutford Ice Stream, that flow into the Weddell Sea (Figure 1). An indicator of lithospheric mantle temperature, Pn velocity provides a useful constraint on geothermal heat flow (e.g., Black & Braile, 1982). Geothermal heat flow, which influences ice-sheet basal lubrication, is an important boundary condition for the modeling of ice sheet dynamics and evolution (e.g., Larour et al., 2012; Pollard et al., 2005; Seroussi et al., 2017).

Additionally, because accurate predictions of glacial isostatic adjustment (GIA) and geoid changes are heavily reliant upon estimates of mantle viscosity, improved constraints on uppermost mantle structure in WANT are also necessary to further improve models of ice-sheet-solid Earth interactions (e.g., Barletta et al., 2018; Groh et al., 2012; Nield et al., 2018; Powell et al., 2020). Considering the accelerating ice mass loss throughout much of WANT (e.g., Shepherd et al., 2019), accurate measurements of geothermal heat flow and GIA-induced solid earth deformation are crucial in evaluating the future stability and evolution of the West Antarctica Ice Sheet (e.g., Whitehouse et al., 2019). The Pn-velocities that we report are the first such observations made within parts of central WANT that are undergoing rapid ice mass loss resulting from climate change (e.g., Holland et al., 2019; Shepherd et al., 2019).

2. Background

2.1. Tectonic Setting

West Antarctica (WANT) is regarded as an assemblage of four discrete crustal blocks, the Antarctic Peninsula (AP), Marie Byrd Land (MBL), Thurston Island-Eights Coast (TIE), and Haag-Ellsworth-Whitmore (HEW), with the HEW being separated from the other blocks by the West Antarctic Rift System (WARS) (Dalziel & Elliot, 1982) (Figure 1). The central portion of the Amundsen Sea Embayment (ASE) sits at the junction of the WARS and two crustal blocks—MBL and the TIE (Figure 1). While the HEW block is considered an allochthonous continental fragment (Dalziel, 2007; Grunow et al., 1987; Jordan et al., 2017; Randall & Mac Niocaill, 2004; Schopf, 1969), MBL, TIE, and the AP developed as fore-arc and magmatic-arc terranes along the paleo-Pacific convergent margin of Gondwana (e.g., Dalziel, 1992). The four crustal blocks of WANT moved away from the East Antarctica Craton during the first WARS extensional phase between ~105 and 85 Ma (e.g., Siddoway, 2008). The WARS continued extending until ~84 Ma, when seafloor spreading between WANT and Zealandia commenced (e.g., Siddoway, 2008). At present, the WARS does not appear to be actively extending (e.g., Donnellan & Luyendyk, 2004; Winberry & Anandakrishnan, 2003); GPS measurements and associated modeling indicate that vertical and horizontal bedrock motions in the ASE are dominated by GIA associated with extensive recent ice mass loss (Barletta et al., 2018; Groh et al., 2012) (Figure 1).

The Ellsworth Mountains are situated in the Ellsworth-Whitmore Mountains province of the HEW, a composite crustal block located west of the Weddell Sea Rift System (Figures 1 and 2). The Haag Nunataks province, located adjacent to the Ellsworth Mountains, is considered part of the HEW (e.g., Jordan et al., 2017) (Figures 1 and 2). The HEW is a geologically and geophysically distinct crustal block within WANT (Schopf, 1969). While the AP, TIE, and MBL crustal blocks were all perturbed, to varying degrees, by deformation and magmatism from the Paleozoic through the Cenozoic (e.g., Jordan et al., 2020), internal deformation within the HEW ceased after the Permo-Triassic Gondwanide orogeny (e.g., Curtis, 2001). Prior to the breakup of Gondwana, the HEW underwent translation and rotation to its current position (e.g., Jordan et al., 2017; Schopf, 1969). Although not internally deformed during the major Cretaceous WARS extensional phase, the HEW underwent ~4 km of uplift during the early Cretaceous (Fitzgerald & Stump, 1991). The HEW sits on thicker crust (30–40 km) compared to the other WANT crustal blocks (An et al., 2015; Chaput et al., 2014; Dunham et al., 2020; O'Donnell et al., 2019; Ramirez et al., 2016, 2017; Shen et al., 2018), but isostatic compensation calculations indicate that the crust is too thin to solely support present elevations in the HEW (Chaput et al., 2014). Several seismic studies have imaged high upper mantle velocities beneath much of the HEW block (Lloyd et al., 2015, 2020; Lucas et al., 2020; O'Donnell et al., 2019; Shen et al., 2018). In addition to high velocities, Lucas et al. (2020) also imaged a low velocity region at depths >200 km beneath the central portion of the HEW indicative of warm upper mantle material and argued that the warm upper mantle may provide some thermal support for present elevations in the HEW.

The eastern portion of MBL is located within the ASE (Figure 1). MBL is a high elevation region, likely supported by upwelling low-density mantle associated with alkaline volcanism beginning ~28–30 Ma (LeMasurier & Landis, 1996). MBL hosts 18 large, subaerial basalt-trachyte shield volcanoes, including Mount Takahe (LeMasurier & Landis, 1996). The source of Cenozoic alkaline volcanism in MBL is debated—many studies hypothesize that a mantle plume fed the Cenozoic volcanism (e.g., Hansen et al., 2014; Heeszel et al., 2016; Lloyd et al., 2020; O'Donnell et al., 2019; Panter et al., 1997; Weaver et al., 1994), while
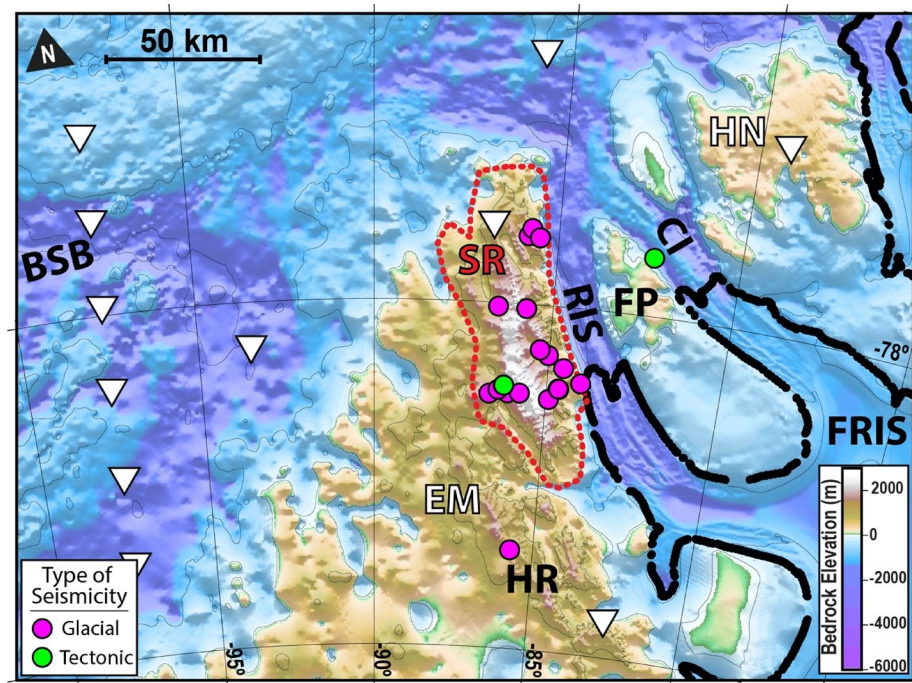
Figure 2. Bedrock topography map of the Ellsworth Mountains (EM) region. The grounding line is delineated in black (Morlighem et al., 2020). The red dashed line outlines the Sentinel Range (SR). Seismic station locations are marked with inverted white triangles. Other abbreviated geographic features: HN: Haag Nunataks, BSB: Byrd Subglacial Basin, HR: Heritage Range, RIS: Rutford Ice Stream, FRIS: Filchner-Ronne Ice Shelf, FP: Fletcher Promontory, CI: Carson Inlet Glacier.

others attribute magmatism to mantle flow induced by the break-up of the slab associated with premid Cretaceous subduction in MBL (e.g., Finn et al., 2005). Consistent with an upper mantle thermal anomaly, widespread slow upper mantle seismic velocities have been imaged beneath MBL and other regions of WANT (Heeszel et al., 2016; Lloyd et al., 2020; Lucas et al., 2020; O'Donnell et al., 2019; Ramirez et al., 2017; Shen et al., 2018; White-Gaynor et al., 2019), with deep low-velocity features that span the mantle transition zone (Emry et al., 2015). Using seismograms from a 2012 magnitude 5.6 earthquake in MBL, O'Donnell et al. (2017) obtained a regional lithospheric mantle V_{Pn} of ~8.0 km/s beneath the WARS and MBL. Within the MBL, crustal seismicity has been attributed to ongoing magmatism at numerous locations (Lough, 2014; Lough et al., 2013; Winberry & Anandakrishnan, 2003).

Along with the Pine Island Glacier (PIG) region, the Hudson Mountains, a Neogene volcanic province characterized by three large, extensively eroded stratovolcanoes, is located in the ASE sector of the TIE crustal block (Rowley et al., 1990) (Figure 1). There is evidence of a recent (207 BCE ± 240 years) volcanic eruption in the Hudson Mountains (Corr & Vaughan, 2008). Although Neogene volcanism may be associated with TIE extension (e.g., Jordan et al., 2010), it has also been attributed to an extension of MBL magmatism beneath the TIE (Hole & LeMasurier, 1994). Consistent with this hypothesis, a number of studies have imaged low seismic velocities extending from MBL toward PIG at upper mantle depths (25–400 km depth) (Heeszel et al., 2016; Lloyd et al., 2015, 2020; Lucas et al., 2020; O'Donnell et al., 2019; Shen et al., 2018) and upper mantle anisotropy in the ASE, measured by shear-wave splitting, is consistent with radial flow from the MBL region (Accardo et al., 2014). Additionally, Kalberg and Gohl (2014) attributed a high-velocity layer identified at the base of the lower crust beneath the ASE continental margin to magma flow from the MBL region.

Seismic imaging suggests the lithosphere throughout much of the WARS has not been perturbed since the formative Jurassic-Cretaceous rifting (Heeszel et al., 2016; Lloyd et al., 2015, 2020; Lucas et al., 2020; O'Donnell et al., 2019; Shen et al., 2018). However, evidence of localized Cenozoic rifting within the WARS

has been noted for the Pine Island Rift (PIR), located beneath PIG, the Terror Rift, and portions of the Bentley Subglacial Trench and Byrd Subglacial Basin (e.g., Clow et al., 2012; Golynsky et al., 2018; Granot et al., 2010, 2013; Lloyd et al., 2015; Lucas et al., 2020; O'Donnell et al., 2019). Granot et al. (2013) argued that regions of localized Cenozoic rifting may represent Eocene-Oligocene transcurrent faults that were reactivated by mid-Miocene to recent extension.

2.2. Glaciologic Setting

Our study area encompasses several major central WANT glacial systems, including the Thwaites Glacier (TG), Pine Island Glacier (PIG), and Rutford basins (Figures 1 and 2). Numerous tributary glaciers situated in the Ellsworth Mountains flow into the TG, PIG, and Rutford basins (Figure 2). While TG and PIG are both marine-terminating glaciers that drain into the ASE, the Rutford Ice Stream is one of the main contributors to the Filchner-Ronne Ice Shelf (King, 2009).

Over the past several decades, TG and PIG have both undergone significant ice mass loss, grounding-line retreat, and thinning (Mouginot et al., 2014; Rignot et al., 2019; Shepherd et al., 2019). The current TG grounding zone can be subdivided into distinct eastern, central, and western regimes that flow into a buttressed and confined ice shelf, an unconfined ice shelf, and a mélange of icebergs and sea ice, respectively (e.g., Fürst et al., 2016; MacGregor et al., 2012; Mouginot et al., 2014). Although glacial bed conditions beneath the West Antarctic Ice Sheet are generally poorly known, there is evidence that TG is underlain by a spatially variable bed (e.g., Muto et al., 2019). Compared to TG, PIG has a larger and more coherent ice shelf, where a number of upstream tributaries channel ice into the central trunk, which travels along a deep subglacial trough that flows into the Pine Island Bay (e.g., Stenoien & Bentley, 2000).

The Ellsworth Mountains are broadly characterized by longitudinal mountain ridges separated by glacier-filled basins (e.g., Sugden et al., 2017). Some glaciers flow west out of the Ellsworth Mountains over the Ellsworth Subglacial Highlands toward the ASE. These glaciers span a complex hydrological network, including two major subglacial lakes, across the Ellsworth Subglacial Highlands (e.g., Rivera et al., 2015; Siegert et al., 2004). Other glaciers originating in the Ellsworth Mountains flow east and eventually merge with the Rutford Ice Stream, which flows over a range of subglacial landforms, including mega-scale glacial lineations, drumlins, and hummocks, into the Filchner-Ronne Ice Shelf (King et al., 2016). Unlike the ASE, the ice mass of the Filchner-Ronne Ice Shelf and associated glaciers has remained relatively stable over the past few decades (Rignot et al., 2019).

2.3. WANT Seismicity

Although limited by sparse seismic station coverage, previous studies have found evidence of tectonic, glacial, and volcanic seismicity in central WANT (e.g., Lough, 2014; Lough et al., 2013; Olinger et al., 2019; Smith, 2006; Winberry & Anandakrishnan, 2003; Winberry et al., 2020). Along with numerous small earthquakes ($M_L < 1$), Winberry and Anandakrishnan (2003) identified larger ($M_L > 2$) earthquakes in two geographic clusters, one in the northern WARS and a second within the WARS interior. Lough (2014) compiled a comprehensive Antarctic seismicity catalog for 2009–2010. Similar to the Winberry and Anandakrishnan (2003) study, Lough (2014) reported minimal tectonic seismicity within the WARS. Lough (2014) also identified both tectonic and volcanic seismicity throughout WANT, with a notable majority of the seismicity clustered in MBL. Within MBL, Lough et al. (2013) identified a swarm of deep (near Moho depth) long-period seismic events, which was interpreted as an active subglacial magmatic complex beneath the youngest subaerial volcanoes in the Executive Committee Range. Aside from the isolated clusters of tectonic seismicity in the WARS (Winberry & Anandakrishnan, 2003) and magmatic seismicity in MBL (Lough, 2014; Lough et al., 2013), prior studies have suggested sparse seismicity in WANT.

While studies of earthquakes and volcano seismicity have been limited by relatively sparse seismic station coverage in central WANT, studies of glacial seismicity have been even more limited. Smith (2006) identified swarms of microseismic activity at the ice-bed interface in a small passive seismic survey on Rutford Ice
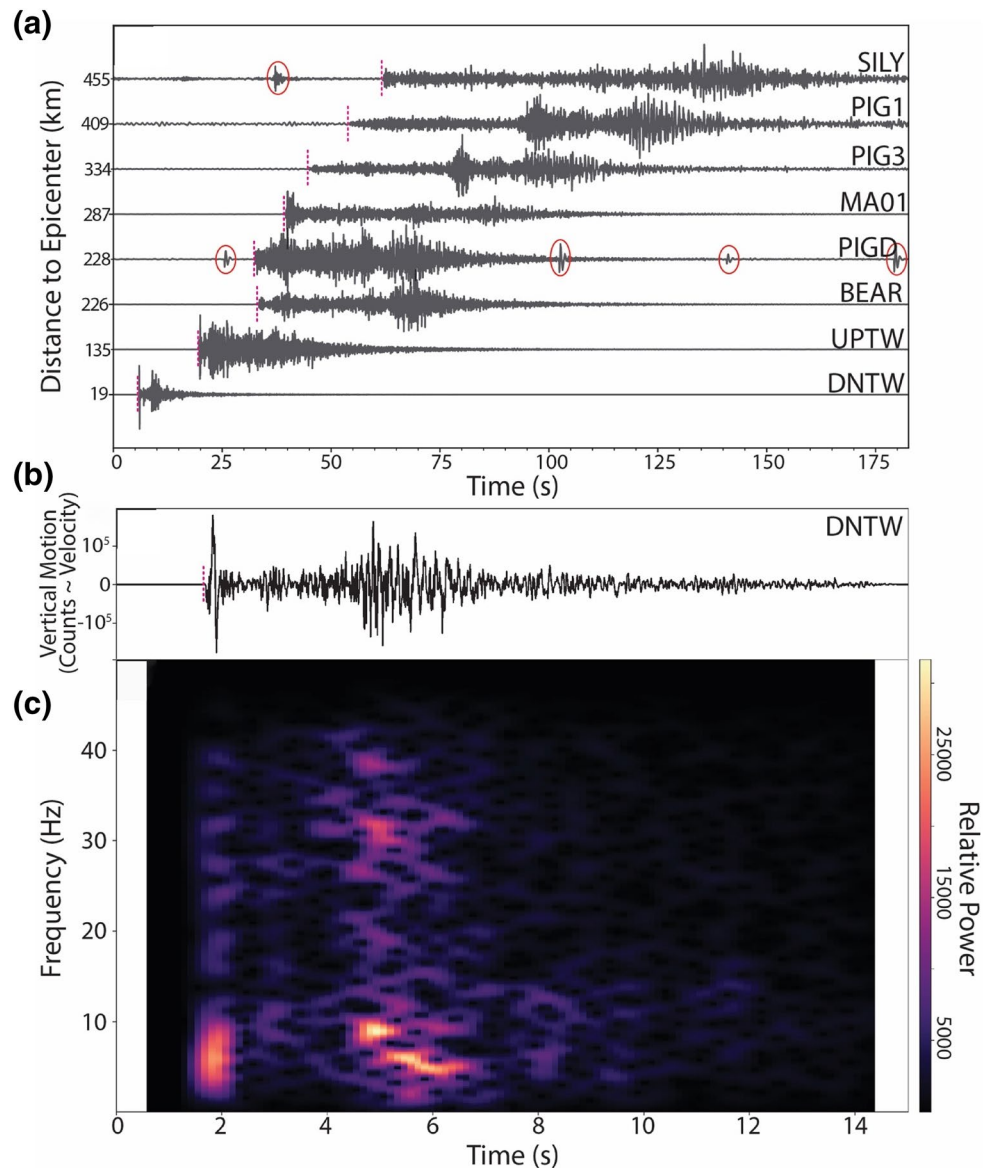
Figure 4. (a) Vertical component seismogram record section from the M_L 3.5, 13 March 2017 earthquake beneath TG (Figure 1). The event origin time corresponds to time zero of the record section. Seismograms are bandpass filtered at 1–20 Hz. The seismograms are labeled on the right with their respective station codes. Icequakes recorded at PIGD and SILY are circled in red. The P-wave arrivals are marked with pink dashed lines. (b) Vertical component seismogram recorded at seismic station DNTW from the March 13, 2017 earthquake beneath TG. (c) Spectrogram of waveform plotted in (b).

Stream. Within the ASE, Olinger et al. (2019) and Winberry et al. (2020) identified near-ice front seismicity that increased notably prior to large glacial calving events at PIG and TG, respectively.

3. Central WANT Seismicity

This study utilizes broadband seismic data collected by the Antarctic portion of the Polar Earth Observing Network (POLENET/ANET; https://doi.org/10.7914/SN/YT_2007) and the UK Antarctic Network (UKANET; https://doi.org/10.7914/SN/1D_2016) (Figure 1). We use data from Polar Earth Observing Network (POLENET) backbone stations and from the US/UK mini array (MA) (Figure 1). The MA extended
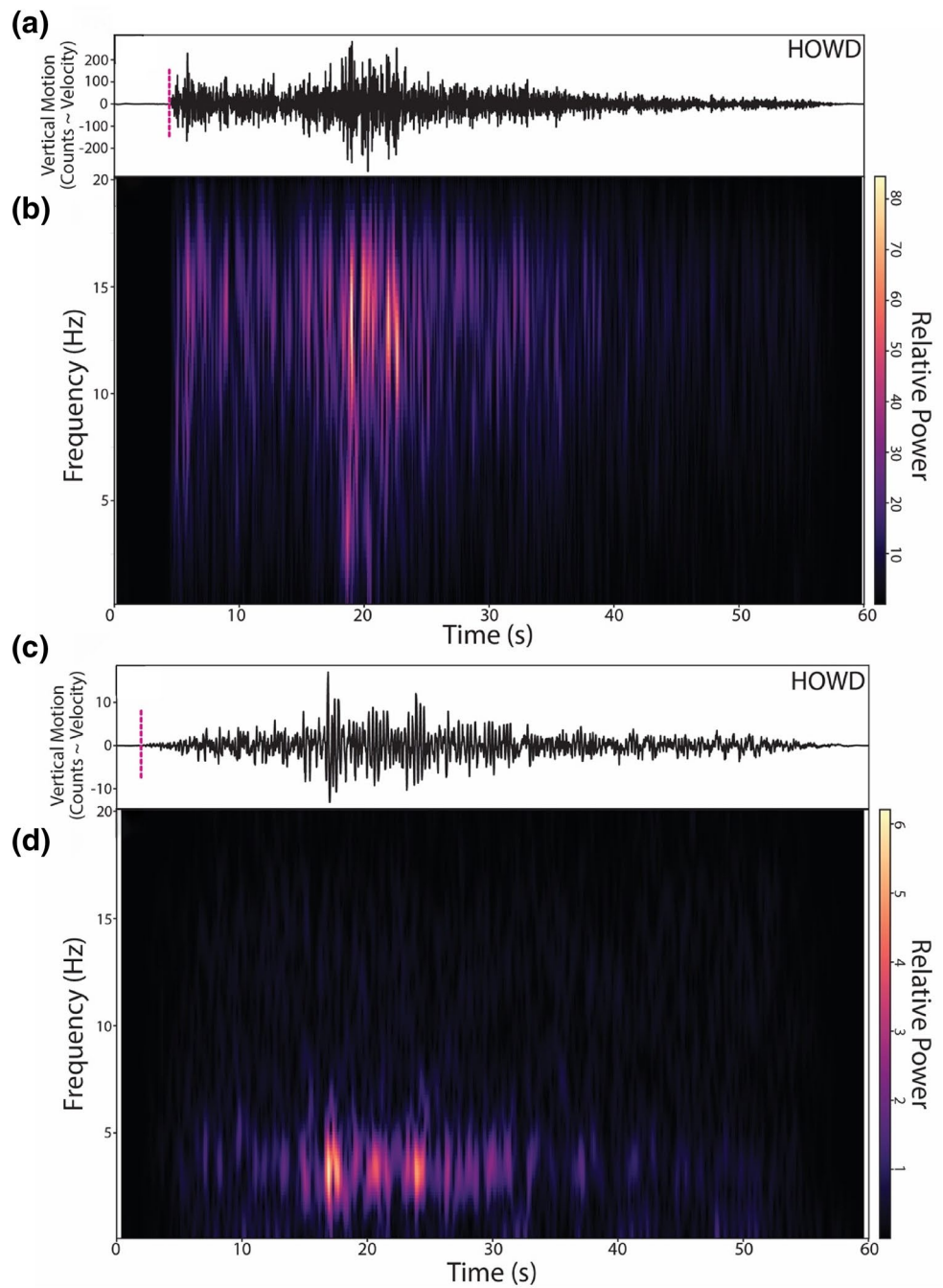
Figure 3. Earthquake and icequake signal comparison using events from the Ellsworth Mountains: (a)–(b) Seismogram and spectrogram from a May 10, 2016, M_L 1.6 earthquake. (c)-(d) Seismogram and spectrogram from a June 1, 2016, M_L 1.9 icequake. The seismograms are filtered with a 1.2 Hz high-pass filter. Pink dashed lines mark the P-wave arrivals.

from the Byrd Subglacial Basin to the Amundsen Sea and consisted of 10 POLENET stations deployed from 2015 to 2016 and 10 UKANET stations deployed from 2016 to 2017, with roughly 70 km composite interstation spacing (Figure 1). This study primarily focuses on the 2-year time interval (2015–2017) during which the MA was deployed and encompasses the region from −80° to −72° latitude and −120° to −75° longitude.

We detected and associated seismic events in central WANT using the Antelope software package by manually picking clear P- and S-wave arrivals with typical traveltime picking errors estimated to be ∼0.1–0.2 s and ∼0.5 s for P- and S-wave arrivals, respectively. We located seismic events with P-wave arrivals on four or more seismic stations using the Hypoinverse earthquake location software (Klein, 2002) with local velocity models (Table S1, S2). The local velocity models used include an ice sheet layer interpolated from BedMachine (Morlighem et al., 2020), where appropriate, and are based on previous studies of shear wave velocity structure and crustal thickness in West Antarctica (e.g., Dunham et al., 2020; Shen et al., 2018). To estimate seismic event magnitudes consistent with previous WANT seismicity studies (e.g., Lough, 2014; Lough et al., 2013), we calculate a local magnitude (M_L) for each seismic event using the equation $M_L = \log\left(\dfrac{A}{T}\right) + 2.76\log\left(Dist\right) - 2.48$, where A is the amplitude in microns of the waveforms sampled at period T and $Dist$ is the distance between source and receiver in kilometers.

Through this process we identified and located 117 seismic events in central WANT, with local magnitudes (M_L) ranging from 1.1 to 3.5 (Table S3). Of the 117 seismic events, 99 were located in the ASE and 18 were located in the Ellsworth Mountains (Figures 1, 2, 7, and 8). Within the ASE, the seismic events are predominantly clustered in the TG and PIG regions and at Mount Takahe (Figure 1). Compared to seismic event locations, which are constrained with an average horizontal location error of ∼1.8 km, event depths are often poorly constrained due to the ray path geometry, with depth location errors ranging from ∼1 to ∼33 km. Well-constrained seismic event depths generally indicate the inclusion of S-wave arrival times and the presence of nearby stations in the event location process.

Seismicity could conceivably arise from glacial, tectonic, or volcano-tectonic processes within central WANT. To interpret event types, we investigated source depths, which discriminate tectonic or volcano-tectonic events at crustal depths from glacial events, and evaluated seismogram characteristics. Traditional earthquake-location methods, including Hypoinverse, provide a standard error associated with depth estimates based on linearized covariance propagation using the least-squares solution. The linearized least-squares solution is subject to the characteristics of the local error minimum. To assess this, we calculated the arrival time misfit for a grid of depths to constrain best-fitting source depths (supporting information S2, S3, and S4). In evaluating waveform characteristics, we examined the seismic spectrum, given that both tectonic and volcanic sources tend to be characterized by broader frequency content than glacial events (supporting information S1) (e.g., Aster & Winberry, 2017; McNutt, 2005; West et al., 2010).

3.1. Seismicity in the Ellsworth Mountains

We located 18 seismic events ($1.1 \leq M_L \leq 2.1$) in the Ellsworth Mountains (Figures 1 and 2), and assessed that 16 of these are likely of glacial origin (Table S3). Glacial seismicity is predominantly confined to a cluster in the southern portion of the Sentinel Range (Figures 1 and 2) and exhibits a maximum spectral amplitude at 1–5 Hz (Figures 3c and d, Supp. Info. S1a). Given our seismic station configuration, we cannot discriminate the source mechanisms of the glacial processes responsible for the activity, however, it can most likely be attributed to glacial stick-slip motion or near-surface ice fracturing in the glacial systems on either side of the Sentinel Range.

We also identified and located two seismic events of inferred tectonic origin in the Ellsworth Mountains. The first earthquake (February 9, 2013; M_L 1.3) is located in the Sentinel Range at ∼8 km depth, and the second earthquake (May 10, 2016; M_L 1.6) is located near the Fletcher Promontory at ∼6 km depth (Figure 2; supporting information S2; Table S3). Both of the Ellsworth Mountains earthquakes exhibit broad spectral content (1–18 Hz; Figures 3a and b; supporting information S1a). We attempted to constrain focal mechanism solutions for these earthquakes, but were unable to usefully do so because of limited seismic station and ray path coverage. Tectonic seismicity observed in the Ellsworth Mountains may be associated with the underlying tectonic stress regime and/or the influence of GIA-induced stress, noting that seismicity has been attributed to postglacial rebound in both Fennoscandia and the Laurentide region (e.g., Keiding et al., 2015; Steffen et al., 2012). Both of the earthquakes are located in the northern portion of the HEW, a region characterized by horst and graben bedrock structures, indicative of rifting (e.g., Doake et al., 1987; Garrett et al., 1987). Considering that the Ellsworth Mountains are currently undergoing ∼5 mm/year of

uplift due to late Pleistocene deglaciation in Antarctica (Argus et al., 2011) and the horst and graben structures provide a zone of preexisting tectonic weakness, the earthquakes can likely be attributed to both underlying tectonic stress and GIA-induced stress in the HEW.

3.2. Earthquake Beneath Thwaites Glacier

The largest seismic event (M_L = 3.5) identified in this study occurred on March 13, 2017 in the TG region, ∼20 km west of the seismic station DNTW (Figures 1 and 4). We find a best-fitting source depth of ∼19 km using Hypoinverse, indicating that the hypocenter is in the middle to lower crust (Supp. Info. S3). Given the proximity of the seismic event to the DNTW seismic station (Figure 1, supporting information S5), we also estimate source depth using the traveltime difference between the S- and P-wave arrivals at DNTW. We find a traveltime difference of 3.069 s between the S- and P-wave arrivals, which corresponds to a source depth of ∼20 km. Using the FOCMEC first-motion program (Snoke, 2003), we obtained a focal mechanism that indicates normal faulting with approximately east-west nodal planes (Figure 1, supporting information S6). Although this earthquake may be attributed to the tectonic background stress regime, it could also be associated with stress reflecting rapid ice mass loss and GIA in the ASE. Notably, the orientations of the nodal planes are consistent with the orientation of horizontal GIA-related bedrock motion in the ASE (Barletta et al., 2018) (Figure 1). This interpretation is analogous to that of present-day seismicity in Greenland which has been, in part, correlated to regions undergoing recent ice mass loss (Olivieri & Spada, 2014). In addition to occurring in deglaciated regions (i.e., Fennoscandia) we may expect that GIA-induced seismicity occurs concurrently with active partial ice mass unloading. Considering the accelerating ice mass loss and retreat of the TG (e.g., Shepherd et al., 2019) and the weak ASE upper mantle and rapid crustal uplift (Barletta et al., 2018; Groh et al., 2012), this earthquake could thus have resulted from GIA-induced stress accumulation.

3.3. Seismicity at Mount Takahe

We located eight seismic events, with source depths of 9–19 km (supporting information S4), beneath the edifice of Mount Takahe, a young (<0.3 Ma) trachytic shield volcano near the western boundary of the TG catchment (Figure 1, Table S3) (e.g., Palais et al., 1988; LeMasurier & Rex, 1990). These events range in magnitude from M_L 1.6–2.5 (Table S3). Considering the location, frequency content (1–10 Hz), and well-constrained source depths, the Mount Takahe events likely arise from volcano-tectonic processes (Figures 1 and 5, supporting information S1b, S4, S7). Due to relatively sparse seismic station coverage around Mount Takahe (Figure 1), we cannot reliably differentiate seismic events of volcano-tectonic origin from those of purely magmatic origin. However, based on evidence of eruptive activity at Mount Takahe within the past 40,000 years (e.g., LeMasurier & Rex, 1990; Palais et al., 1988), it is possible that a number of events, if not all, can be attributed to magmatic processes.

Further, in addition to the eight well-recorded events, we identified 17 additional events likely located at Mount Takahe using cross-correlation analysis (Table S4). The aforementioned additional events are only recorded at one or two of the nearest seismic stations; therefore, we cannot determine reliable source locations. Considering the nearest seismic station, DNTW, is located ∼125 km away from Mount Takahe, lower magnitude seismicity associated with this seismic activity likely remains undetected. Seismicity has been attributed to subglacial magmatism at a number of volcanoes in MBL (Lough, 2014; Lough et al., 2013; Winberry & Anandakrishnan, 2003), and Lough (2014) located two events, likely of volcanic or volcano-tectonic origin, near Mount Takahe. In investigating volcanic and volcano-tectonic seismicity in this region, this study has been limited by sparse seismic station coverage (Figure 1). We note that since Mount Takahe is at the western border of the TG catchment (Figure 1), subglacial volcanic activity may have a long-term impact on the evolution and stability of TG.

3.4. Glacial Seismicity in the Central ASE

We located 91 intermediate-frequency (1–4 Hz) seismic events of glacial origin in the ASE during 2015–2017 (Figures 1 and 6–8). These seismic events exhibit impulsive P-wave arrivals and range in magnitude
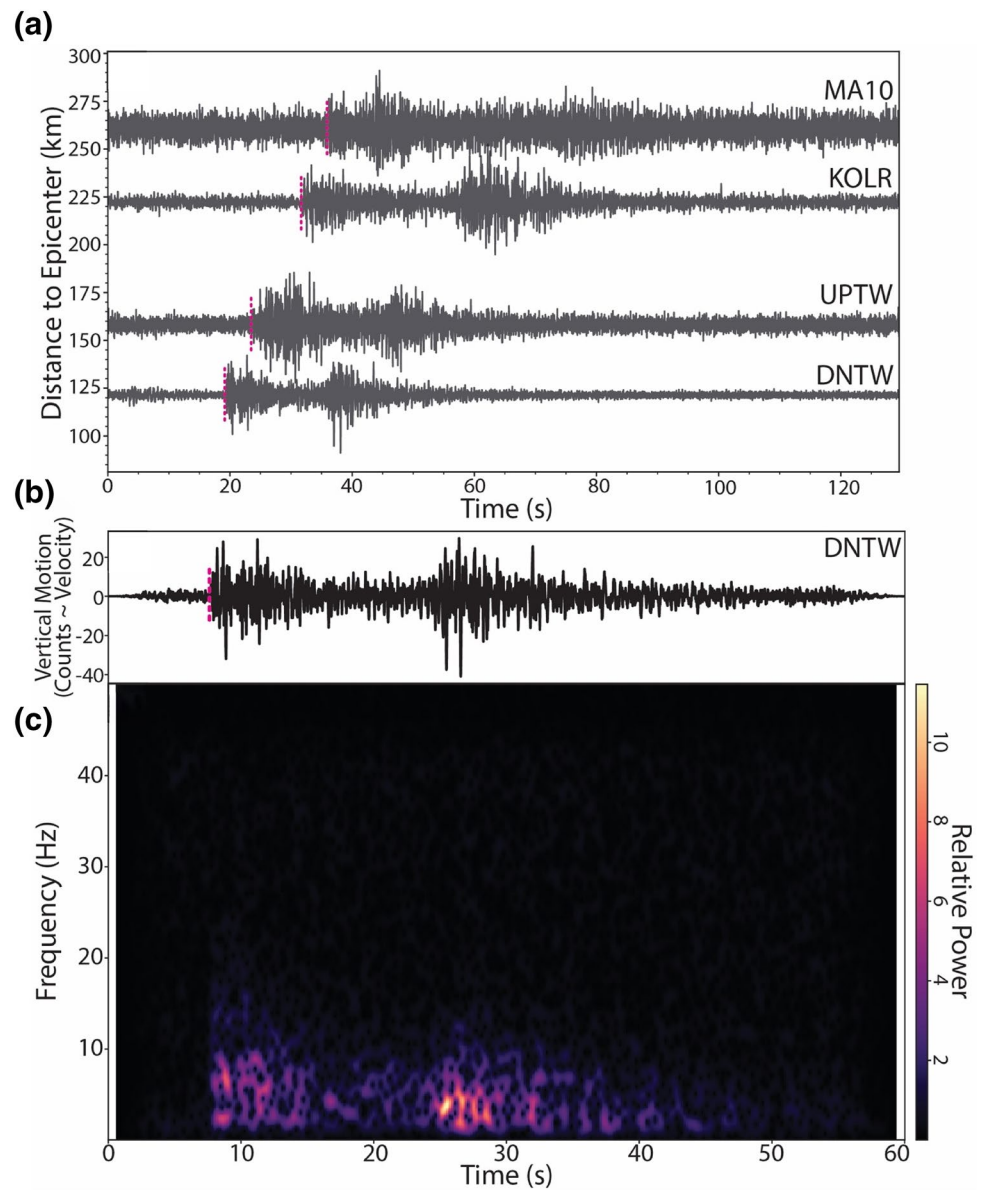
Figure 5. (a) Vertical component seismogram record section from the August 16, 2016, M_L 1.6 seismic event near Mount Takahe. The event origin time corresponds to time zero of the record section. Seismograms are filtered with a 1.5 Hz high-pass filter. The seismograms are labeled on the right with their respective station codes. P-wave arrivals are marked with pink dashed lines. (b) Vertical component seismogram from the August 16, 2016 event recorded at seismic station DNTW. (c) Spectrogram of waveform plotted in (b).

from M_L 1.1–3.2, with an average M_L of ∼ 2. The events are predominantly clustered in two regions. The first cluster is located at the western portion of the TG grounding zone (Figures 1 and 7), and the second cluster is located at the grounding zone of the PIG glacier (Figures 1 and 8). We find that the majority of the events in this population occur in the days preceding and following major calving events in the ASE (supporting information S9 and S10). While we focus on the best-recorded events here, we note that many more events were observable at the closest one or two seismic stations, both preceding and following the aforementioned calving events.

We identified a number of long-period seismic events, likely produced by ice calving, originating from the western terminus of the TG in early July 2017 (supporting information S8a, S9). To confirm the calving at
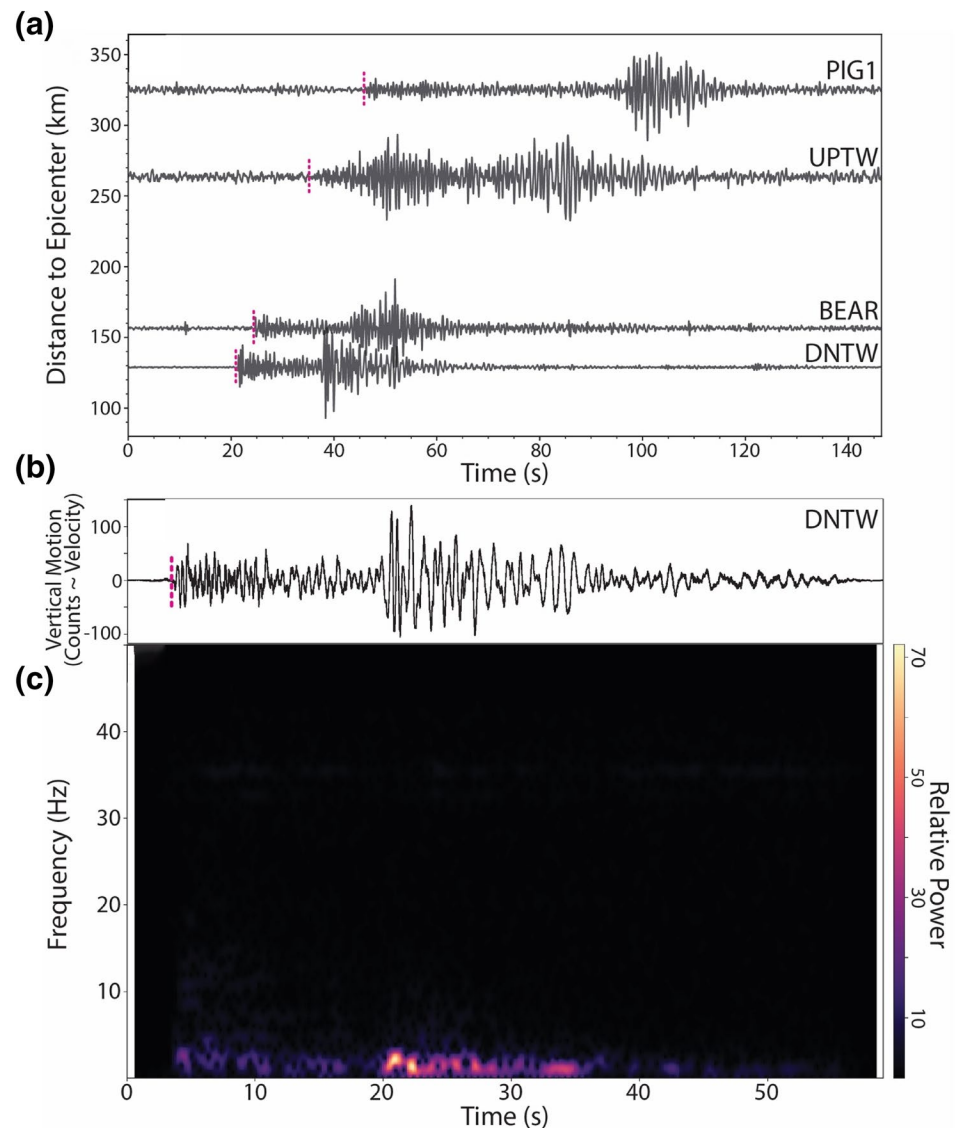
Figure 6. (a) Vertical component seismogram record section from a June 29, 2017, M_L 1.6 icequake in the TG region. The event origin time corresponds to time zero of the record section. Seismograms are filtered with a 0.8 Hz high-pass filter. The seismograms are labeled at right with their respective station codes. Pink dashed lines mark the P-wave arrivals. (b) Vertical component seismogram of the June 29, 2017 icequake recorded at seismic station DNTW. (c) Spectrogram of waveform plotted in (b).

TG, we compared Sentinel-1 imagery captured on July 2, 2017 and July 4, 2017 (Figures 7b–7e). Consistent with the timing of the long-period seismic event, we find that significant calving activity occurred in the western portion of the TG between July 2, 2017 and July 4, 2017 (Figures 7b–7e). The July 2017 calving activity was accompanied by a substantial increase in discrete intermediate-frequency icequakes predominantly located in the region of TG calving (Figures 7b–7e; supporting information S9; Table S3). The long-period seismic events identified in this study are similar to three seismic events studied by Winberry et al. (2020) near the same portion of the TG terminus on April 10, 2017 and November 8, 2018. Using both seismic data and optical imagery, the Winberry et al. (2020) study similarly correlated the long-period seismic events to calving activity at TG.

We also observe an increase in discrete intermediate-frequency glacial seismicity at the grounding zone of PIG that is, likely related to a series of PIG calving events, characterized by ~11 long-period seismic events
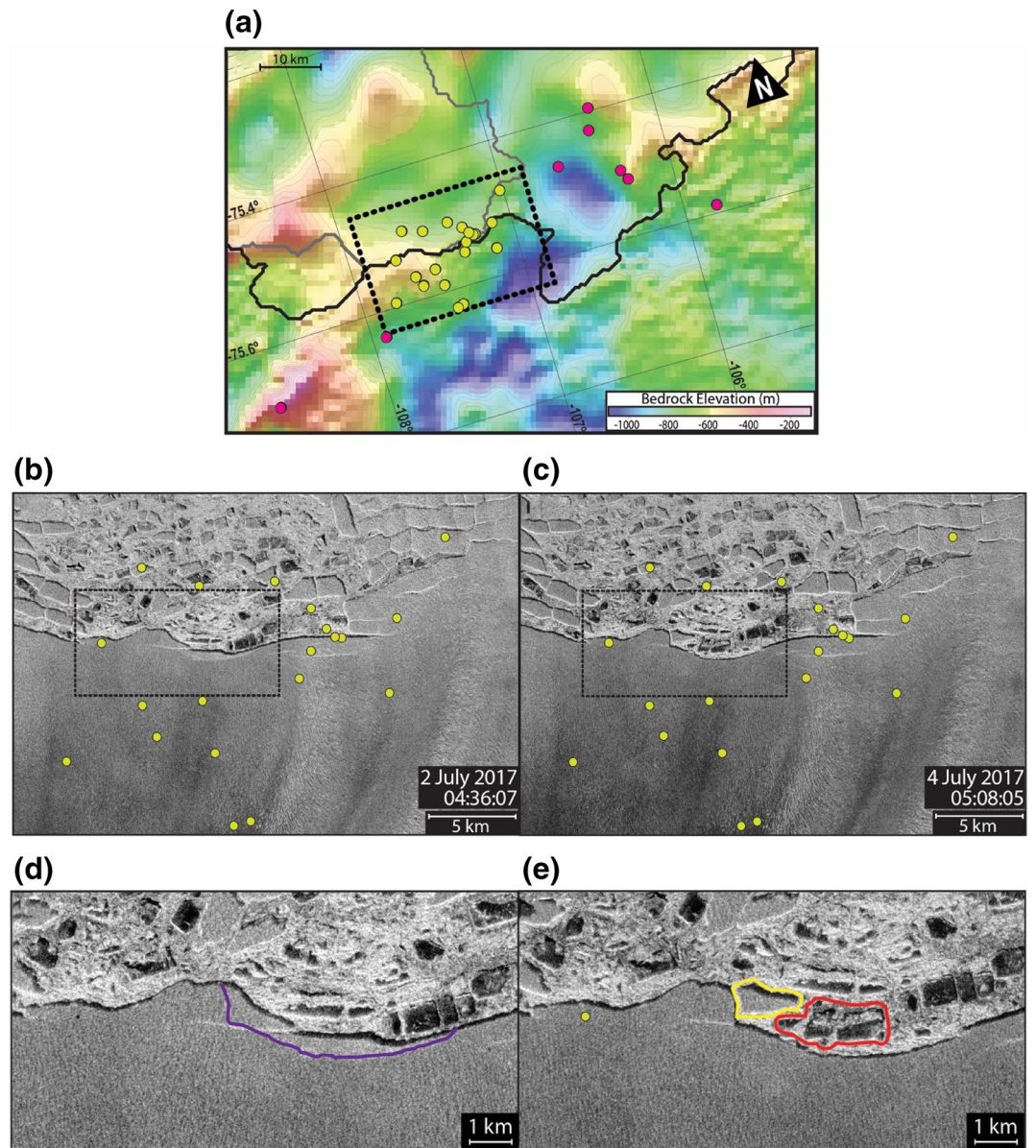
Figure 7. (a) Western TG grounding zone bedrock topography (Morlighem et al., 2020). The black and gray lines delineate the grounding line and ice front positions, respectively (Morlighem et al., 2020). Icequake locations are demarcated with pink and yellow circles. The location of the imagery in (b)-(c) is marked by a black dashed line. (b)-(c) Sentinel-1 imagery showing the evolution of the ice front associated with the July 2017 calving activity. The location of imagery in figures (d)-(e) is marked with a black dotted line. (d)-(e) Sentinel-1 imagery of a zoomed-in region of the western TG ice front captured on July 2, 2017 (d) and July 4, 2017 (e). (d) The solid purple line indicates the TG terminus position on July 2, 2017. (e) The yellow and red polygons outline a newly-calved iceberg and capsized icebergs, respectively.

(supporting information S8b), that occurred in February 2016 (Figures 1 and 8; supporting information S10). Sentinel-1 imagery acquired on February 1, 2016 and February 26, 2016 is used to confirm the calving activity (Figures 8b and c). While the high frequency icequakes are primarily located near and slightly upstream of the PIG grounding zone, it should be noted that the events are distinctly inland (by up to many 10s of km) of the calving front (Figure 8).

Overall, we find that the intermediate-frequency icequakes are predominantly located at or near the grounding zone of either TG or PIG and occur preceding and following time intervals of significant calving
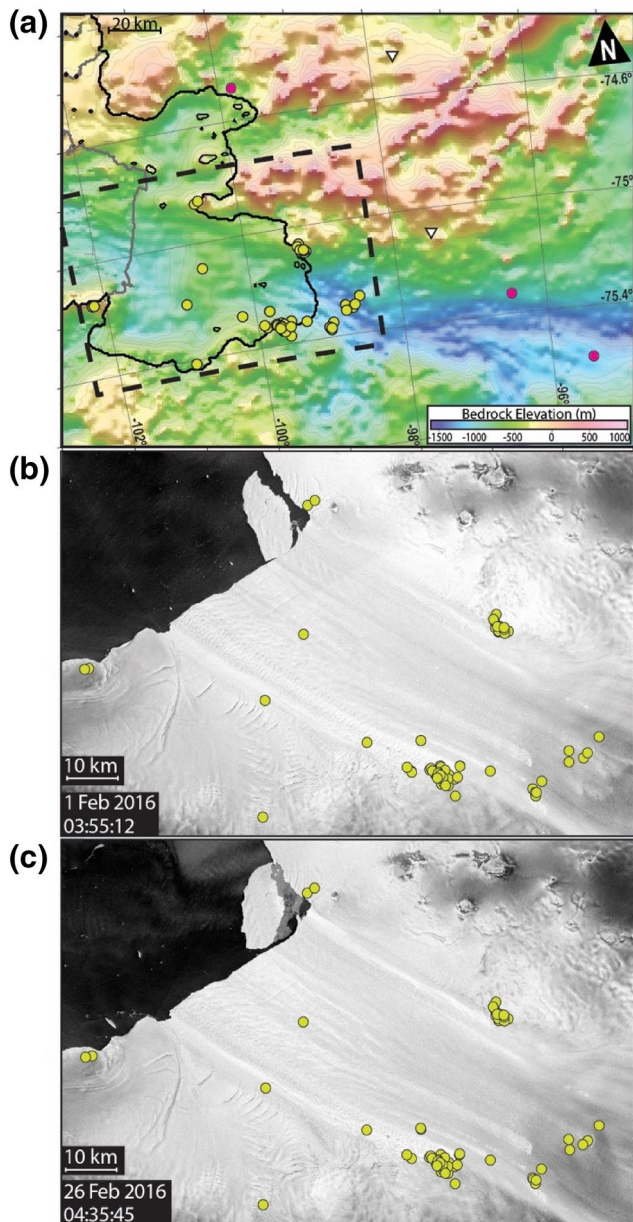
Figure 8. (a) PIG regional bedrock topography (Morlighem et al., 2020). The black and gray lines delineate the grounding line and ice front positions, respectively (Morlighem et al., 2020). Icequake locations are demarcated with pink and yellow circles. The location of the imagery in (b)-(c) is delineated with black dashed line. (b)-(c) Sentinel-1 imagery showing the evolution of the ice front associated with the February 2016 calving activity at PIG.

activity (Figures 1, 7 and 8; supporting information S9 and S10). Winberry et al. (2020) also identified an increase in discrete, intermediate-frequency icequake activity at the western terminus of the TG prior to the November 8, 2018 and April 10, 2017 calving activity, however, they did not locate the events. Calving events are inherently characterized by the propagation of fractures (e.g., Benn et al., 2007); therefore, the temporal correlation between calving activity and glacial seismicity arising from fracture propagation is natural. While the Winberry et al. (2020) study attributes the seismicity preceding TG calving activity to elevated rates of fracture propagation in the region of incipient tabular iceberg formation, the icequakes located in this study cannot be wholly attributed to processes associated with the formation of incipient tabular icebergs and must therefore be generated by other glacial processes (Figures 1, 7, and 8). Additionally, the majority of PIG icequakes are not located at or near the terminus and, therefore, cannot be attributed to iceberg formation processes (Figures 1 and 8). Given the temporal association with major calving events, waveform characteristics, and proximity to the grounding zone, the majority of icequakes located in this study could arise from subglacial, englacial, and/or subaerial fracture development and propagation (Figures 1, 6, 7, and 8; supporting information S1b, S9, and S10).

4. Uppermost Mantle Structure

We investigated uppermost mantle structure in the Ellsworth Mountains and central ASE using Pg- and Pn-wave arrivals from the seismic events discussed above. Pg-waves travel only through the crust, while Pn-waves are refracted along the crust-mantle boundary (e.g., Beghoul et al., 1993; Menke & Richards, 1980), traveling (1) from a seismic source through the crust to the mantle, (2) through the uppermost mantle (the mantle lid), and (3) from the mantle back through the crust to the surface. We determine the mean regional Pg and Pn velocities for both the Ellsworth Mountains and the central ASE by fitting travel times to a straight line as a function of epicentral distance (Figure 9). In addition to determining the mean regional Pn velocity for the central ASE, we also use the Pn arrival times to image lateral variations in the ASE uppermost mantle velocity using the tomography method of Hearn (1996) in areas where ray coverage is sufficient (Figure 10; supporting information S11 and S12). Although S-wave travel times are used to locate many of the seismic events, Sg and Sn velocities are not estimated in this study due to sparse data coverage.

For the Ellsworth Mountains, Pg and Pn-wave arrivals from 18 well-recorded seismic events, including events of both glacial and tectonic origin (Figures 1 and 2), yield 78 P-wave first arrivals recorded at distances between 14 and 284 km. The Pg and Pn traveltime branches are clearly evident in the traveltime plot, with a crossover distance of ∼180 km (Figure 9a), consistent with a mean crustal thickness of 38 km and with prior estimates of crustal thickness (An et al., 2015; Chaput et al., 2014; Dunham et al., 2020; O'Donnell et al., 2019; Ramirez et al., 2017, 2016; Shen et al., 2018). Based on the above Pg-Pn crossover distance, we classify 33 of the 78 P-wave arrivals as Pn arrivals (Figure 9a).

For the central ASE, Pg and Pn-wave arrivals from 46 well-recorded glacial events yield 290 P-wave first arrivals recorded between 37 and 490 km (Figures 1 and 9b). Both Pg and Pn traveltime branches are evident in the traveltime plot, corresponding to a Pg-Pn crossover distance of ∼143 km (Figure 9b), which is con-
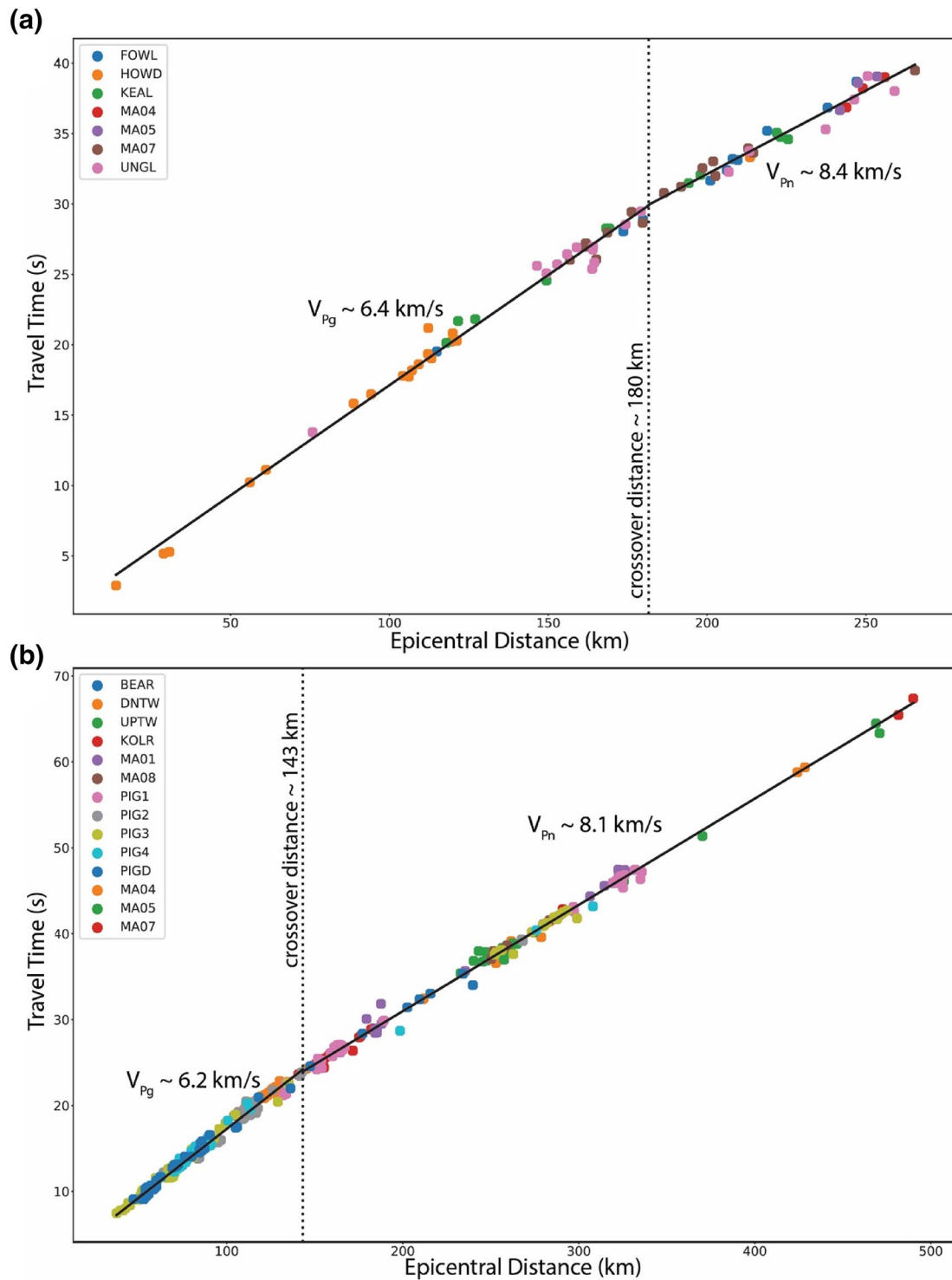
Figure 9. (a) Travel times versus epicentral distance for seismic events located in the Ellsworth Mountains. We differentiated Pn arrivals from Pg arrivals based on a crossover distance of ~180 km. We fit the Pg and Pn data with a least-squares straight-line to determine an average Pg and Pn velocity of ~6.40 ± 0.02 km/s and ~8.40 ± 0.03 km/s, respectively. (b) Travel times versus epicentral distance for seismic events of glacial origin located in the central ASE. We differentiated Pn arrivals from Pg arrivals based on a crossover distance of ~143 km. We fit the Pg and Pn data with a least-squares straight-line to determine an average Pg and Pn velocity of ~6.20 ± 0.02 km/s and ~8.10 ± 0.01 km/s, respectively.
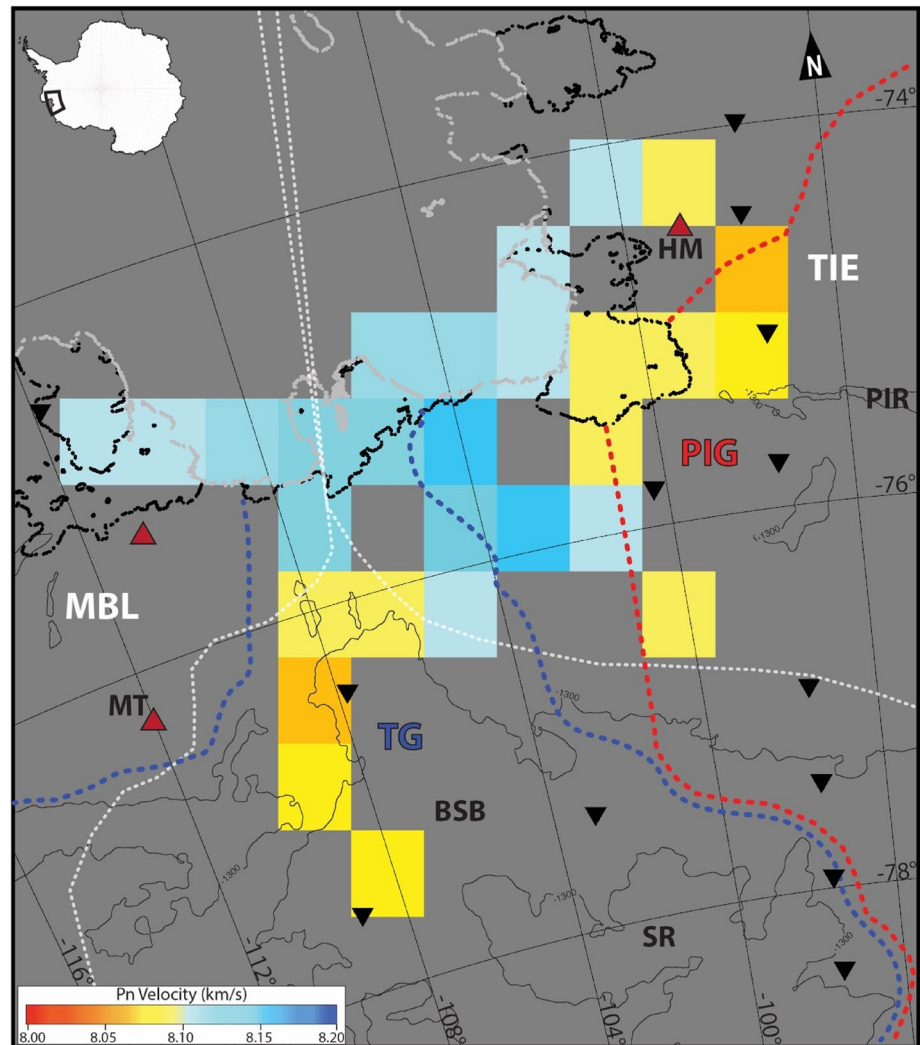
Figure 10. Pn velocity tomography model of the central ASE. The grounding line and ice front position are delineated by black and gray lines, respectively (Morlighem et al., 2020). Inverted black triangles mark the locations of seismic stations. MBL and the TIE crustal block are outlined by dashed white lines. The Thwaites Glacier catchment (TG) and Pine Island Glacier (PIG) catchment are outlined in blue and red dashed lines, respectively. Thin black lines contour the −1,300 m bedrock elevation. Red triangles mark the locations of subaerial Cenozoic volcanoes (LeMasurier & Thomson, 1990). Other abbreviated geographic features: BSB: Byrd Subglacial Basin, SR: Sinuous Ridge, PIR: Pine Island Rift; MT: Mount Takahe; HM: Hudson Mountains.

sistent with a mean crustal thickness of 25 km (An et al., 2015; Dunham et al., 2020; O'Donnell et al., 2019; Ramirez et al., 2017, 2016; Shen et al., 2018). Based on the Pg-Pn crossover distance, we classify 151 of the 290 P-wave first arrivals as Pn arrivals (Figure 9b).

4.1. Pn Inversion Method

Using the tomography method of Hearn (1996), we inverted Pn-wave traveltime residuals to obtain an uppermost mantle velocity model for the central ASE. The traveltime, t_{ij}, of the ray traveling between seismic event j and station i is described by

$$t_{ij} = a_i + b_j + \sum d_{ijk} \left(s_k \right)$$

where a_i and b_j are the crustal static delays for station i and event j, d_{ijk} is the distance traveled by ray ij in mantle cell k, and s_k is the slowness perturbation for cell k (Hearn 1994, 1996). We assumed azimuthal isotropy in this study and anisotropy terms are thus not included in the traveltime equation. In the Hearn (1996) method, a regularized least-squared algorithm (Paige & Saunders, 1982) iteratively solves for mantle-lid slowness (s_k), and for station (a_i), and event (b_j) delays.

The surface of the uppermost mantle was gridded into 80 km × 80 km cells, and Laplacian (second-order) regularization was applied (Paige & Saunders, 1982). The cell size was selected to ensure multiple ray paths within each cell (supporting information S12). The Laplacian regularization weighting parameter controls the trade-off between data misfit and resolution (Aster et al., 2018; Hearn, 1996). We chose a damping value of 150 in our inversion, which provided acceptable resolution width and error size (supporting information S13). Additionally, we required a minimum hit count of five rays per grid cell; cells not meeting this requirement were shaded gray in the associated figures (Figure 10; supporting information S12).

4.1.1. Pn Inversion Results and Resolution

Pn inversion results are shown in Figure 10, and estimated uncertainties are shown in Figure 11. The range of Pn velocity across the model is about 0.1 km/s, and the average standard deviation is 0.04 km/s, estimated from 100 bootstrap iterations with replacement (Hearn & Ni, 1994; Koch, 1992). The highest uncertainties (~0.13 km/s) are found near the grounding line of TG and can likely be attributed to hypocentral location errors associated with sparse seismic station coverage (Figure 11).

A synthetic model is used to evaluate the effects of raypath coverage on spatial resolution (supporting information S14). We built the synthetic model with the same event-station pairs used in the tomographic inversion of the true data (supporting information S14a). Gaussian noise was added to the synthetic traveltimes with a standard deviation of 0.45 s, equivalent to the root-mean-square residual from the actual inversion. We find that input synthetic anomalies are well recovered, although subdued in magnitude, after inverting the synthetic test model using the same parameters as for the real traveltime data (supporting information S14b).

For simplicity, we assume that all glacial events are located at 1 km depth in our inversion. Given the unconstrained possible glacial seismic source mechanisms, event depth could feasibly vary between 0 km and ~2 km. To assess the dependence of the Pn velocity model on glacial event depths, we ran Pn inversions for a range of realistic depths (0, 1, and 2 km). We did not find any significant dependence between glacial source depth and the Pn velocity model (supporting information S15).

4.2. Discussion of Uppermost Mantle (Pn) Velocities

Pn-wave velocities are often used to infer the thermal and tectonic history and conditions of the lithospheric mantle. Lateral Pn velocity variations can be attributed to changes in mantle temperature, composition, and/or pressure. While uppermost mantle velocities can vary significantly, the average Pn velocity of continental lithospheric mantle is ~8.0 km/s (e.g., Mooney et al., 2002). Tectonically stable mantle lids are characterized by higher Pn velocities (>8.0 km/s), while lower Pn velocities (<7.8 km/s) can indicate thermal anomalies and the possible presence of partial melt (e.g., Hearn & Ni, 1994; Schutt et al., 2018). Because seismic velocities are primarily influenced by temperature at upper mantle depths (e.g., Black & Braile, 1982; Faul & Jackson, 2005; Goes et al., 2000), V_{Pn} variability can be used to estimate variations in uppermost mantle temperature in central WANT. Following the Goes et al. (2000) temperature-velocity relationship indicating that a 100 K temperature anomaly corresponds to a 0.5%–2% P-wave velocity anomaly, we calculate minimum temperature changes assuming the lowest end member in this range.

After regressing the traveltime data from the 18 well-recorded seismic events in the Ellsworth Mountain region, we find a mean regional Pn velocity of 8.40 ± 0.03 km/s and a Pg velocity of 6.40 ± 0.02 km/s, where the uncertainty is the standard deviation of the regression (Figure 9a). With such a high average regional Pn velocity, the Ellsworth Mountains are likely underlain by a cool, tectonically stable mantle lid. Consistent with this study, Ramirez et al. (2017), Shen et al. (2018), and O'Donnell et al. (2019) also imaged fast veloc-
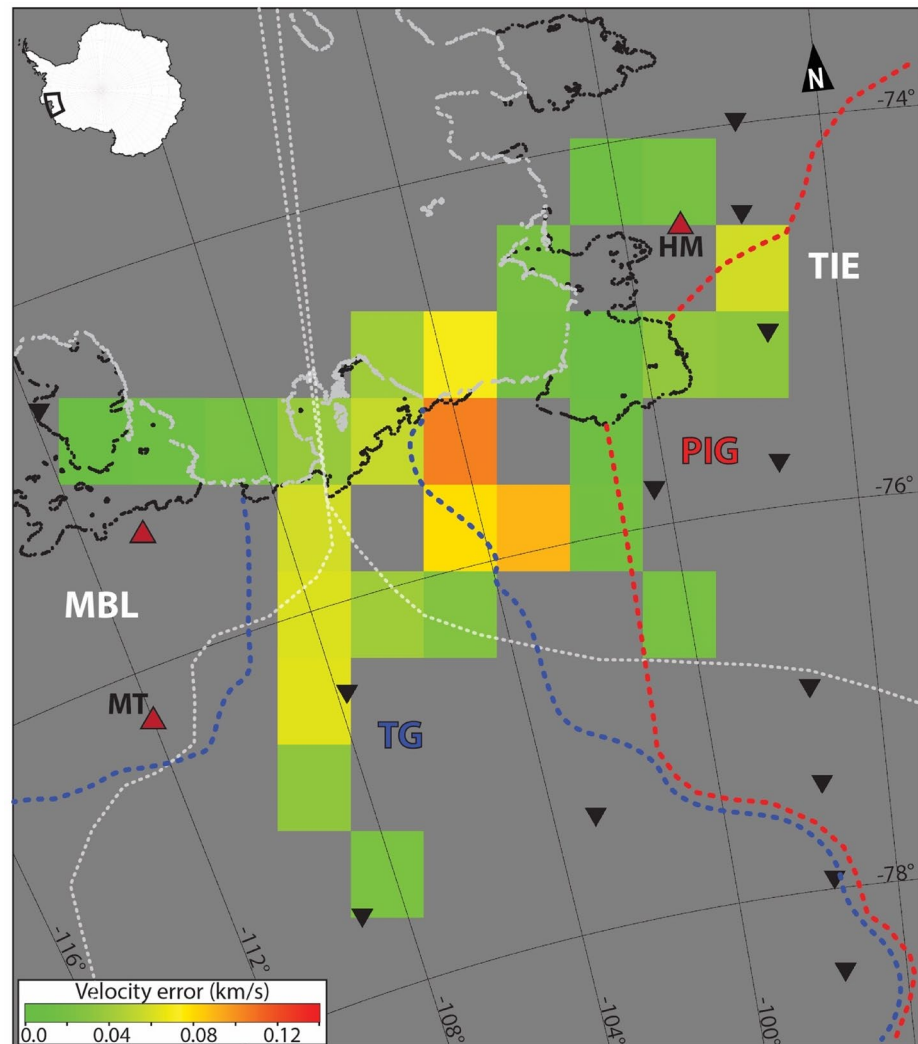
Figure 11. Standard deviations of Pn velocities computed from bootstrap analysis. Inverted black triangles mark the locations of seismic stations. MBL and the TIE crustal block are outlined by dashed white lines. The Thwaites Glacier (TG) and Pine Island Glacier (PIG) catchments are outlined in blue and red dashed lines, respectively. Red triangles mark the locations of subaerial Cenozoic volcanoes (LeMasurier & Thomson, 1990). Other abbreviated geographic features: MT: Mount Takahe; HM: Hudson Mountains.

ities at uppermost mantle depths beneath the Ellsworth Mountains. The high uppermost mantle velocity is consistent with tectonic quiescence in the HEW following the Jurassic extension of the Weddell Sea Rift System (e.g., Riley et al., 2020).

For the central ASE, regression of the traveltime data yields a mean Pn velocity of 8.09 ± 0.01 km/s and a Pg velocity of 6.20 ± 0.02 km/s (Figure 9b). The small uncertainty in the mean Pn velocity is consistent with the small range in Pn velocities of 8.05–8.18 km/s obtained from the tomographic inversion (Figure 10). Compared to Pn velocities (∼8.0–8.1 km/s) in the interior of TG (∼−76.0°, −108.0°) and in the PIG region (∼−75.0°, −98.0°), slightly higher Pn velocities (∼8.1–8.18 km/s) are imaged near the grounding line of TG, and at the boundary of the MBL and TIE crustal blocks (∼−75.77°, −107.33°) (Figure 10). After considering the errors associated with the inversion (Figure 11), variations in Pn velocity of ∼0.1 km/s appear to be resolved in the model, but are near the limit of detectability as controlled by limited ray coverage and resolution (Figure 11; supporting information S11, S12, and S14). The indication of slightly higher Pn velocities beneath the terminus of TG compared to lower velocities beneath PIG and the TG interior is consistent with heterogeneous upper mantle structure across the region seen in the Shen et al. (2018),

O'Donnell et al. (2019), Lloyd et al. (2020), and Lucas et al. (2020) upper mantle velocity models. While the crustal thickness in our Pn velocity model is consistent with the crustal thicknesses estimated in Kalberg and Gohl (2014), we do not compare Pn velocities found in this study to the Kalberg and Gohl (2014) velocity model as they do not report Pn velocities.

The velocity transition from higher to slightly lower Pn velocities is located in the same region as the boundary of the MBL and TIE crustal blocks; therefore, a variable lithospheric structure is not unexpected given the disparate geologic histories of the two crustal blocks (e.g., Mukasa & Dalziel, 2000; Pankhurst et al., 1998; Riley et al., 2017; Zundel et al., 2019). Alternatively, variable Pn velocities could indicate that the uppermost mantle underlying PIG and the TG interior has been thermally perturbed to a greater degree than the uppermost mantle beneath the TG terminus region. If Pn velocity variability is attributed to thermal variability, ~50 K hotter uppermost mantle material is expected beneath PIG and the TG interior compared to the TG terminus. This result is consistent with Lucas et al. (2020) who estimated that PIG is underlain by ~55 K hotter upper mantle material compared to TG.

Although there is some indication of variable ASE uppermost mantle structure, overall fast Pn velocities (≥8.05 km/s) indicate a tectonically stable lithospheric mantle. Consistent with this finding, both Shen et al. (2018) and O'Donnell et al. (2019) also report overall fast uppermost mantle shear wave velocities beneath the ASE. Our results thus support the Shen et al. (2018) interpretation that the high uppermost mantle velocities indicate the presence of lithosphere that has cooled significantly since the major Cretaceous phase of WARS rifting (Siddoway, 2008). To explain GPS-constrained ASE GIA uplift, Barletta et al. (2018) showed that a solid Earth viscoelastic model with a 50–60 km thick elastic lithosphere is required. Strong, tectonically stable mantle lithosphere has been correlated with thick elastic lithosphere (e.g., Tesauro et al., 2015); therefore, our Pn results are also broadly consistent with the presence of a 50–60 km thick elastic lithosphere beneath the ASE.

While Pn velocities indicate that both the ASE and Ellsworth Mountains may be underlain by tectonically stable lithospheric mantle, the ASE is characterized by lower Pn velocities (8.1 km/s) compared to the Ellsworth Mountains (8.4 km/s). To compare the Pn velocities between the Ellsworth Mountains and ASE, they first must be corrected for crustal thickness. Assuming a crustal density of 2,750 kg/m^3, the ~25 km thick ASE crust (e.g., O'Donnell et al., 2019) correlates to a pressure of ~675 MPa and the ~38 km thick Ellsworth Mountains crust (e.g., Dunham et al., 2020) correlates to a pressure of ~1,025 MPa. Following Barazangi and Ni (1982), we attribute a 0.1 km/s change in V_{Pn} to 1,000 MPa pressure variability, which implies that only ~0.04 km/s of the 0.3 km/s V_{Pn} difference between the average uppermost mantle velocities beneath the Ellsworth Mountains and ASE can be attributed to a pressure effect. This leaves a ~0.26 km/s difference in Pn velocities between the ASE and the Ellsworth Mountains to be explained by some other mechanism. Additionally, although azimuthal anisotropy may impact Pn velocity estimates in this study, the ~0.26 km/s V_{Pn} variability in central WANT cannot be explained by anisotropy alone.

The ~0.26 km/s V_{Pn} difference between the ASE and Ellsworth Mountains corresponds to a cumulative V_{Pn} anomaly of ~3.2%, similar to the ~4.0% upper mantle P-wave velocity variation between the ASE and Ellsworth Mountains reported by Lucas et al. (2020). While local variations (<80 km) in geothermal heat flow cannot be constrained in this study, we can infer uppermost mantle thermal variability from Pn velocities on a regional scale. The ~3.2% variability in V_{Pn} suggests that the Ellsworth Mountains are underlain by an uppermost mantle that is, at least 160 K cooler than the central ASE. This finding is consistent with Lucas et al. (2020), who estimated ~145 K cooler upper mantle beneath the Ellsworth Mountains compared to the central ASE. Uppermost mantle thermal variability across central WANT is consistent with previous geothermal heat flow estimates that find higher heat flow in the ASE (e.g., Dziadek et al., 2017; Dziadek et al., 2019) compared to the HEW (e.g., Shen et al., 2020). Additionally, thermal variations in the uppermost mantle have significant implications for upper mantle viscosity, which can vary by two orders of magnitude with temperature variations of ±100 K in WANT (O'Donnell et al., 2017). Therefore, our Pn results suggest that uppermost mantle viscosity could vary significantly across the central WANT, which could affect GIA rebound patterns and rates within the central ASE and across central WANT (e.g., Nield et al., 2018).

Previous studies generally attribute higher upper mantle velocities beneath central WANT to lithosphere that has remained unmodified since the Mesozoic rifting of the WARS and lower velocities, such as those

found beneath PIG and portions of the Bentley Subglacial Trench, to lithosphere that has been thermally altered by localized Cenozoic rifting in the WARS (e.g., Lloyd et al., 2015, 2020; Lucas et al., 2020; O'Donnell et al., 2019; Shen et al., 2018). Although we find lower uppermost mantle velocities in the central ASE (~8.1 km/s) compared to the Ellsworth Mountains (~8.4 km/s), actively rifting lithosphere is typically characterized by uppermost mantle velocities that are even lower (<7.8 km/s) than those observed beneath the central ASE. The uppermost mantle velocities found beneath the central ASE do not necessitate the presence of thermally perturbed lithosphere by Cenozoic rifting and instead may simply reflect variations in the thickness of stable continental lithosphere. This conclusion does not preclude the presence of thermally perturbed sublithospheric mantle beneath the ASE and some other parts of WANT argued for by Lloyd et al. (2015), Shen et al. (2018), Lloyd et al. (2020), and Lucas et al. (2020).

5. Summary and Conclusions

We located 117 previously unidentified seismic events, mostly occurring between 2015 and 2017, originating from tectonic, volcano-tectonic, and glacial processes in central WANT. The events are located in the Ellsworth Mountains, at TG and PIG, and beneath Mount Takahe (Figures 1, 2, 7a, and 8a; supporting information S7; Table S3). In central WANT, tectonic seismicity may be attributed to either the underlying tectonic stress regime and/or to GIA-induced stress. We locate a number of events beneath Mount Takahe that are likely of volcano-tectonic origin (Figures 1 and 5; supporting information S7) and note an increase in discrete, intermediate-frequency glacial seismicity preceding and following time intervals of calving activity at TG and PIG (Figures 1, 7, and 8; supporting information S9 and S10). We identify several geographic seismicity clusters within central WANT, but find the WARS to be notably devoid of seismic activity (Figure 1). This corroborates previous studies (e.g., Donnellan & Luyendyk, 2004; Lough, 2014; Winberry & Anandakrishnan, 2003), and further suggests that the rift system is no longer undergoing extension.

Using Pg- and Pn-wave arrivals from a number of seismic events in central WANT, we find that both the Ellsworth Mountains and central ASE are underlain by a relatively fast uppermost mantle (~8.1–8.4 km/s). Fast uppermost mantle velocities throughout central WANT are consistent with the presence of a tectonically stable mantle lid, with the Ellsworth Mountains characterized by distinctly higher Pn velocity (8.4 km/s) compared to the ASE (8.1 km/s), even after crustal thickness differences are accounted for. Fast uppermost mantle velocities throughout central WANT do not support the presence of lithosphere that has been thermally perturbed by localized Cenozoic WARS rifting, as suggested by previous studies, and may simply reflect variations in the thickness of stable continental lithosphere. Although our study region can be characterized by a generally fast uppermost mantle, laterally variable uppermost mantle structure likely impacts both geothermal heat flow and mantle rheology in central WANT.

Data Availability Statement

All seismic data utilized in this study can be obtained from the IRIS Data Management Center (www.iris.edu), and all satellite imagery can be obtained from the European Space Agency (ESA) (https://scihub.copernicus.eu/) and the U.S. Geological Survey (USGS) (https://earthexplorer.usgs.gov) data centers.

References

Accardo, N. J., Wiens, D. A., Hernandez, S., Aster, R. C., Nyblade, A. A., Huerta, A., et al. (2014). Upper mantle seismic anisotropy beneath the West Antarctic Rift System and surrounding region from shear wave splitting analysis. *Geophysical Journal International*, *198*(1), 414–429. https://doi.org/10.1093/gji/ggu117

An, M., Wiens, D. A., Zhao, Y., Feng, M., Nyblade, A., Kanao, M., et al. (2015). S-velocity model and inferred Moho topography beneath the Antarctic Plate from Rayleigh waves. *Journal of Geophysical Research: Solid Earth*, *120*, 359–383. https://doi.org/10.1002/2014JB011332

Argus, D. F., Blewitt, G., Peltier, R., & Kreemer, C. (2011). Rise of the Ellsworth Mountains and parts of the East Antarctic Coast observed with GPS. *Geophysical Research Letters*, *38*, L16303. https://doi.org/10.1029/2011GL048025

Aster, R. C., Thurber, & Borchers, C. H. B. (2018). *Parameter estimation and inverse problems* (3rd ed.) Elsevier.

Aster, R. C., & Winberry, J. P. (2017). Glacial seismology. *Reports on Progress in Physics*, *80*, 126801. https://doi.org/10.1088/1361-6633/aa8473

Barazangi, M., & Ni, J. (1982). Velocities and propagation characteristics of Pn and Sn waves beneath the Himalayan Arc and Tibetan Plateau: Possible evidence for underthrusting of Indian continental lithosphere beneath Tibet. *Geology*, *10*(4), 179–185. http://doi.org/10.1130/0091-7613(1982)10<179:VAPCOP>2.0.CO;2

Barletta, V. R., Bevis, M., Smith, B. E., Wilson, T. J., Brown, A., Bordoni, A., et al. (2018). Observed rapid bedrock uplift in Amundsen Sea Embayment promotes ice-sheet stability. *Science*, *360*(6395), 1335–1339. https://doi.org/10.1126/science.aao1447

Beghoul, N., Barazangi, M., & Isacks, B. L. (1993). Lithospheric structure of Tibet and western North America: Mechanisms of uplift and a comparative study. *Journal of Geophysical Research*, *98*(B2), 1997–2016. https://doi.org/10.1029/92JB02274

Benn, D. I., Warren, C. R., & Mottram, R. H. (2007). Calving processes and the dynamics of calving glaciers. *Earth-Science Reviews*, *82*, 143–179. https://doi.org/10.1016/j.earscirev.2007.02.002

Black, P. R., & Braile, L. W. (1982). Pn velocity and cooling of the continental lithosphere. *Journal of Geophysical Research*, *87*(B13). https://doi.org/10.1029/JB087iB13p10557

Chaput, J., Aster, R. C., Huerta, A., Sun, X., Lloyd, A. D., Wiens, D., et al. (2014). The crustal thickness of West Antarctica. *Journal of Geophysical Research: Solid Earth*, *119*(1), 378–395. https://doi.org/10.1002/2013jb010642

Clow, G., Cuffey, K., & Waddington, E. (2012). *High heat-flow beneath the central portion of the west Antarctic ice sheet*. San Francisco, CA: American Geophysical Union Fall Meeting.

Corr, H., & Vaughan, D. (2008). A recent volcanic eruption beneath the West Antarctic ice sheet. *Nature Geoscience*, *1*, 122–125. https://doi.org/10.1038/ngeo106

Curtis, M. L. (2001). Tectonic history of the Ellsworth Mountains, West Antarctica: Reconciling a Gondwana enigma. *The Geological Society of America Bulletin*, *113*(7), 939–958. https://doi.org/10.1130/0016-7606(2001)113<0939:THOTEM>2.0.CO;2

Dalziel, I. W. D. (1992). Antarctica; a tale of two supercontinents? *Annual Review of Earth and Planetary Sciences*, *20*(1), 501–526. https://doi.org/10.1146/annurev.ea.20.050192.002441

Dalziel, I. W. D. (2007). The Ellsworth Mountains: Critical and enduringly enigmatic. *International symposium on Antarctic Earth sciences*. U.S. Geological Survey and The National Academies. https://doi.org/10.3133/of2007-1047.srp004

Dalziel, I. W. D., & Elliot, D. H. (1982). West Antarctica: Problem child of Gondwanaland. *Tectonics*, *1*(1), 3–19. https://doi.org/10.1029/tc001i001p00003

Doake, C. S. M., Crabtree, R. D., & Dalziel, I. W. D. (1987). Sub-glacial morphology between Ellsworth Land and Antarctic Peninsula. In R. L. Oliver, P. R. James, & J. B. Jago (Eds.), *Antarctic Earth science* (pp. 270–273). Canberra: Australian Academy of Science.

Donnellan, A., & Luyendyk, B. P. (2004). GPS evidence for a coherent Antarctic plate and for postglacial rebound in Marie Byrd Land. *Global and Planetary Change*, *42*(1), 305–311. https://doi.org/10.1016/j.gloplacha.2004.02.006

Dunham, C. K., O'Donnell, J. P., Stuart, G. W., Brisbourne, A. M., Rost, S., Jordan, T. A., et al. (2020). A joint inversion of receiver function and Rayleigh wave phase velocity dispersion data to estimate crustal structure in West Antarctica. *Geophysical Journal International*, *223*(3), 1644–1657. https://doi.org/10.1093/gji/ggaa398

Dziadek, R., Gohl, K., Diehl, A., & Kaul, N. (2017). Geothermal heat flux in the Amundsen Sea sector of West Antarctica: New insights from temperature measurements, depth to the bottom of the magnetic source estimation, and thermal modeling. *Geochemistry, Geophysics, Geosystems*, *18*, 2657–2672. https://doi.org/10.1002/2016GC006755

Dziadek, R., Gohl, K., & Kaul, N. (2019). Elevated geothermal surface heat flow in the Amundsen Sea Embayment, West Antarctica. *Earth and Planetary Science Letters*, *506*, 530–539. https://doi.org/10.1016/j.epsl.2018.11.003

Emry, E. L., Nyblade, A. A., Julià, J., Anandakrishnan, S., Aster, R. C., Wiens, D. A., et al. (2015). The mantle transition zone beneath West Antarctica: Seismic evidence for hydration and thermal upwellings. *Geochemistry, Geophysics, Geosystems*, *16*(1), 40–58. https://doi.org/10.1002/2014gc005588

Faul, U. H., & Jackson, I. (2005). The seismological signature of temperature and grain size variations in the upper mantle. *Earth and Planetary Science Letters*, *234*(1), 119–134. https://doi.org/10.1016/j.epsl.2005.02.008

Finn, C. A., Müller, R. D., & Panter, K. S. (2005). A Cenozoic diffuse alkaline magmatic province (DAMP) in the southwest Pacific without rift or plume origin. *Geochemistry, Geophysics, Geosystems*, *6*. https://doi.org/10.1029/2004GC000723

Fitzgerald, P. G., & Stump, E. (1991). Early Cretaceous uplift of the Ellsworth Mountains, West Antarctica. *Science*, *254*, 92–94.

Fürst, J. J., Durand, G., Gillet-Chaulet, F., Tavard, L., Rankl, M., Braun, M., et al. (2016). The safety band of Antarctica ice shelves. *Nature Climate Change*, *6*, 479–484. https://doi.org/10.1038/nclimate2912

Garrett, S. W., Herrod, L. D. B., & Mantripp, D. R. (1987). Crustal structure of the area around the Haag Nunataks, West Antarctica: New aeromagnetic and bedrock elevation data. In G. D. McKenzie (Ed.), Gondwana six: Structure, tectonics, and geophysics, geophysical monograph series (Vol. 40, pp. 109–115). Washington, DC: American Geophysical Union.

Goes, S., Govers, R., & Vacher, P. (2000). Shallow mantle temperatures under Europe from P and S wave tomography. *Journal of Geophysical Research*, *105*(B5), 11153–11169. https://doi.org/10.1029/1999JB900300

Golynsky, A. V., Ferraccioli, F., Hong, J. K., Golynsky, D. A., von Frese, R. R. B., Young, D. A., et al. (2018). New magnetic anomaly map of the Antarctic. *Geophysical Research Letters*, *45*, 6437–6449. https://doi.org/10.1029/2018GL078153

Granot, R., Cande, S. C., Stock, J. M., & Damaske, D. (2013). Revised Eocene-Oligocene kinematics for the West Antarctic rift system. *Geophysical Research Letters*, *40*, 279–284. https://doi.org/10.1029/2012GL054181

Granot, R., Cande, S. C., Stock, J. M., Davey, F. J., & Clayton, R. W. (2010). Postspreading rifting in the Adare Basin, Antarctica: Regional tectonic consequences. *Geochemistry, Geophysics, Geosystems*, *11*(8). https://doi.org/10.1029/2010GC003105

Groh, A., Ewert, H., Scheinert, M., Fritsche, M., Rülke, A., Richter, A., et al. (2012). An investigation of Glacial Isostatic Adjustment over the Amundsen Sea sector, West Antarctica. *Global and Planetary Change*, *98–99*, 45–53. https://doi.org/10.1016/j.gloplacha.2012.08.001

Grunow, A. M., Dalziel, I. W. D., & Kent, D. V. (1987). Ellsworth-Whitmore Mountains crustal block western Antarctica: New paleomagnetic data and their tectonic significance. In G. D. McKenzie (Ed.), Gondwana six: Structure, tectonics, and geophysics, geophysical monograph series (Vol. 40, pp. 161–172). Washington, DC: American Geophysical Union.

Hansen, S. E., Graw, J. H., Kenyon, L. M., Nyblade, A. A., Wiens, D. A., Aster, R. C., et al. (2014). Imaging the Antarctic mantle using adaptively parameterized P-wave tomography: Evidence for heterogeneous structure beneath West Antarctica. *Earth and Planetary Science Letters*, *408*, 66–78. https://doi.org/10.1016/j.epsl.2014.09.043

Hearn, T. M. (1996). Anisotropic Pn tomography in the western United States. *Journal of Geophysical Research*, *101*, 8403–8414. https://doi.org/10.1029/96JB00114

Hearn, T. M., & Ni, J. F. (1994). Pn velocities beneath continental collision zones: The Turkish-Iranian Plateau. *Geophysical Journal International*, *117*(2), 273–283. https://doi.org/10.1111/j.1365-246X.1994.tb03931.x

Heeszel, D. S., Wiens, D. A., Anandakrishnan, S., Aster, R. C., Dalziel, I. W., Huerta, A. D., et al. (2016). Upper mantle structure of central and West Antarctica from array analysis of Rayleigh wave phase velocities. *Journal of Geophysical Research: Solid Earth*, *121*(3), 1758–1775. https://doi.org/10.1002/2015jb012616

Hole, M. J., & LeMasurier, W. E. (1994). Tectonic controls on the geochemical composition of Cenozoic, mafic alkaline volcanic rocks from West Antarctica. *Contributions to Mineralogy and Petrology*, *117*(2), 187–202. https://doi.org/10.1007/BF00286842

Holland, P. R., Bracegirdle, T. J., Dutrieux, P., Jenkins, A., & Steig, E. J. (2019). West Antarctic ice loss influenced by internal climate variability and anthropogenic forcing. *Nature Geoscience*, *12*, 718–724. https://doi.org/10.1038/s41561-019-0420-9

Jordan, T. A., Ferraccioli, F., & Leat, P. T. (2017). New geophysical compilations link crustal block motion to Jurassic extension and strike-slip faulting in the Weddell Sea Rift System of West Antarctica. *Gondwana Research*, *42*, 29–48. http://doi.org/10.1016/j.gr.2016.09.009

Jordan, T. A., Ferraccioli, F., Vaughan, D. G., Holt, J. W., Corr, H., Blankenship, D. D., et al. (2010). Aerogravity evidence for major crustal thinning under the Pine Island Glacier region (West Antarctica). *The Geological Society of America Bulletin*, *122*(5–6), 714–726. https://doi.org/10.1130/B26417.1

Jordan, T. A., Riley, T. R., & Siddoway, C. S. (2020). The geological history and evolution of West Antarctica. *Nature Reviews Earth Environ*, *1*, 117–133. https://doi.org/10.1038/s43017-019-0013-6

Kalberg, T., & Gohl, K. (2014). The crustal structure and tectonic development of the continental margin of the Amundsen Sea Embayment, West Antarctica: Implications from geophysical data. *Geophysical Journal International*, *198*, 327–341. https://doi.org/10.1093/gji/ggu118

Keiding, M., Kreemer, C., Lindholm, C. D., Gradmann, S., Olesen, O., & Kierulf, H. P. (2015). A comparison of strain rates and seismicity for Fennoscandia: Depth dependency of deformation from glacial isostatic adjustment. *Geophysical Journal International*, *202*, 1021–1028. https://doi.org/10.1093/gji/ggv207

King, E. C. (2009). Flow dynamics of the Rutford Ice Stream ice-drainage basin, West Antarctica, from radar stratigraphy. *Annals of Glaciology*, *50*(51), 42–48. https://doi.org/10.3189/172756409789097586

King, E. C., Hamish, P. D., & Smith, A. M. (2016). Subglacial landforms beneath Rutford Ice Stream, Antarctica: Detailed bed topography from ice-penetrating radar. *Earth System Science Data*, *8*(1), 151–158. https://doi.org/10.5194/essd-8-151-2016

Klein, F. W. (2002). User's guide to HYPOINVERSE–2000, a Fortran program to solve for earthquake locations and magnitudes. *U.S. Geological Survey Open-File Report*, *02*(171), 123. https://pubs.usgs.gov/of/2002/0171/

Koch, M. (1992). Bootstrap inversion for vertical and lateral variations of the S wave structure and the v_p/v_s-ratio from shallow earthquakes in the Rhinegraben seismic zone, Germany. *Tectonophysics*, *210*(1–2), 91–115. https://doi.org/10.1016/0040-1951(92)90130-X

Lander, J. F. (1959). Seismicity of Antarctica. *Earthquake Notes*, *30*, 16–17.

Larour, E., Morlighem, M., Seroussi, H., Schiermeier, J., & Rignot, E. (2012). Ice flow sensitivity to geothermal heat flux of Pine Island Glacier, Antarctica. *Journal of Geophysical Research*, *117*. https://doi.org/10.1029/2012JF002371

LeMasurier, W. E., & Landis, C. A. (1996). Mantle-plume activity recorded by low-relief erosion surfaces in West Antarctica and New Zealand. *The Geological Society of America Bulletin*, *108*(11), 1450–1466. https://doi.org/10.1130/0016-7606(1996)108<1450:MPARBL>2.3.CO;2

LeMasurier, W. E., & Rex, D. C. (1990). Mount Takahe. In W. E. LeMasurier & J. W. Thomson (Eds.), *Volcanoes of the Antarctic plate and southern oceans, Antarctic Research series* (Vol. 48, pp. 169–174). Washington, DC: American Geophysical Union.

Lloyd, A. J., Wiens, D. A., Nyblade, A. A., Anandakrishnan, S., Aster, R. C., Huerta, A. D., et al. (2015). A seismic transect across West Antarctica: Evidence for mantle thermal anomalies beneath the Bentley Subglacial Trench and the Marie Byrd Land Dome. *Journal of Geophysical Research: Solid Earth*, *120*(12), 8439–8460. https://doi.org/10.1002/2015jb012455

Lloyd, A. J., Wiens, D. A., Zhu, H., Tromp, J., Nyblade, A. A., Aster, R. C., et al. (2019). Seismic structure of the Antarctic upper mantle based on adjoint tomography. *Journal of Geophysical Research: Solid Earth*, *124*. https://doi.org/10.1029/2019JB017823

Lough, A. C. (2014). *Studies of seismic sources in Antarctica using an extensive deployment of broadband seismographs Doctoral dissertation)*. St. Louis, MO: Washington University. https://openscholarship.wustl.edu/etd/1319

Lough, A. C., Wiens, D. A., Barcheck, C. G., Anandakrishnan, S., Aster, R. C., Blankenship, D. D., et al. (2013). Seismic detection of an active subglacial magmatic complex in Marie Byrd Land, Antarctica. *Nature Geoscience*, *6*(12), 1031. https://doi.org/10.1038/ngeo1992

Lough, A. C., Wiens, D. A., & Nyblade, A. A. (2018). Reactivation of ancient Antarctica rift zones by intraplate seismicity. *Nature Geoscience*, *11*, 515–519. https://doi.org/10.1038/s41561-018-0140-6

Lucas, E. M., Soto, D., Nyblade, A. A., Lloyd, A. L., Aster, R. C., Wiens, D. A., et al. (2020). P- and S-wave velocity structure of central West Antarctica: Implications for the tectonic evolution of the West Antarctic Rift System. *Earth and Planetary Science Letters*, *546*. https://doi.org/10.1016/j.epsl.2020.116437

MacGregor, J., Catania, G., Markowski, M., & Andrews, A. (2012). Widespread rifting and retreat of ice-shelf margins in the eastern Amundsen Sea Embayment between 1972 and 2011. *Journal of Glaciology*, *58*(209), 458–466. https://doi.org/10.3189/2012JoG11J262

McNutt, S. R. (2005). Volcanic seismology. *Annual Review of Earth and Planetary Sciences*, *32*, 461–491. https://doi.org/10.1146/annurev.earth.33.092203.122459

Menke, W. H., & Richards, P. (1980). Crust-mantle whispering gallery phases: A deterministic model of teleseismic Pn wave propagation. *Journal of Geophysical Research*, *85*, 5416–5422. https://doi.org/10.1029/JB085iB10p05416

Mooney, W. D., Prodehl, C., & Pavlenkova, N. (2002). Seismic velocity structure of the continental lithosphere from controlled source data. *International Geophysics Series*, *81*(A), 887–910.

Morlighem, M., Rignot, E., Binder, T., Blankenship, D., Drews, R., Eagles, G., et al. (2020). Deep glacial troughs and stabilizing ridges unveiled beneath the margins of the Antarctic ice sheet. *Nature Geoscience*, *13*, 132–137. https://doi.org/10.1038/s41561-019-0510-8

Mouginot, J., Rignot, E., & Scheuchl, B. (2014). Sustained increase in ice discharge from the Amundsen Sea Embayment, West Antarctica, from 1973 to 2013. *Geophysical Research Letters*, *41*, 1576–1584. https://doi.org/10.1002/2013GL059069

Mukasa, S. B., & Dalziel, I. W. D. (2000). Marie Byrd Land, West Antarctica: Evolution of Gondwana's Pacific margin constrained by zircon U-Pb geochronology and feldspar common-Pb isotopic compositions. *Geological Society of America Bulletin*, *112*(4), 611–627. https://doi.org/10.1130/0016-7606(2000)112<0611:MBLWAE>2.3.CO;2

Muto, A., Anandakrishnan, S., Alley, R. B., Horgan, H. J., Parizek, B. R., Koellner, S., et al. (2019). Relating bed character and subglacial morphology using seismic data from Thwaites Glacier, West Antarctica. *Earth Planet Science Letters*, *507*, 199–206. https://doi.org/10.1016/j.epsl.2018.12.008

Nield, G. A., Whitehouse, P. L., van der Wal, W., Blank, B., O'Donnell, J. P., & Stuart, G. W. (2018). The impact of lateral variations in lithospheric thickness on glacial isostatic adjustment in West Antarctica. *Geophysical Journal International*, *214*, 811–824. https://doi.org/10.1093/gji/ggy158

Okal, E. A. (1981). Intraplate seismicity of Antarctica and tectonic implications. *Earth and Planetary Science Letters*, *52*, 397–409.

Olinger, S., Denolle, M., & Lipovsky, B. P. (2019). Seismicity generated by rifting and calving at pine Island glacier ice shelf. San Francisco, CA: American Geophysical Union Fall Meeting.

Olivieri, M., & Spada, G. (2014). Ice melting and earthquake suppression in Greenland. *Polar Science*, *9*(1), 94–106. https://doi.org/10.1016/j.polar.2014.09.004

O'Donnell, J. P., Selway, K., Nyblade, A. A., Brazier, R. A., Wiens, D. A., & Anandakrishnan, S. (2017). The uppermost mantle seismic velocity and viscosity structure of central West Antarctica. *Earth and Planetary Science Letters*, *472*, 38–49. https://doi.org/10.1016/j.epsl.2017.05.016

O'Donnell, J. P., Stuart, G. W., Brisbourne, A. M., Selway, K., Yang, Y., & Nield, G. A. (2019). The uppermost mantle seismic velocity structure of West Antarctica from Rayleigh wave tomography: Insights into tectonic structure and geothermal heat flow. *Earth and Planetary Science Letters*, *522*, 219–233. https://doi.org/10.1016/j.epsl.2019.06.024

Paige, C. C., & Saunders, M. A. (1982). LSQR: An algorithm for sparse linear equations and sparse least squares. *ACM Transactions on Mathematical Software*, *8*(1), 43–71. https://doi.org/10.1145/355984.355989

Palais, J. M., Kyle, P. R., McIntosh, W. C., & Seward, D. (1988). Magmatic and phreatomagmatic volcanic activity at Mt. Takahe, West Antarctica, based on tephra layers in the Byrd Ice Core and field observations at Mt. Takahe. *Journal of Volcanology and Geothermal Research*, *35*, 295–317.

Pankhurst, R. J., Weaver, S. D., Bradshaw, J. D., Storey, B. C., & Ireland, T. R. (1998). Geochronology and geochemistry of pre-Jurassic superterranes in Marie Byrd Land, Antarctica. *Journal of Geophysical Research*, *103*(B2), 2529–2547. https://doi.org/10.1029/97JB02605

Panter, K. S., Kyle, P. R., & Smellie, J. L. (1997). Petrogenesis of a phonolite-trachyte succession at Mount Sidley, Marie Byrd Land, Antarctica. *Journal of Petrology*, *38*(9), 1225–1253.

Pollard, D., DeConto, R. M., & Nyblade, A. A. (2005). Sensitivity of Cenozoic Antarctic ice sheet variations to geothermal heat flux. *Global and Planetary Change*, *49*, 63–74. https://doi.org/10.1016/j.gloplacha.2005.05.003

Powell, E., Gomez, N., Hay, C., Latychev, K., & Mitrovica, J. X. (2020). Viscous effects in the solid earth response to modern Antarctic ice mass flux: Implications for geodetic studies of WAIS stability in a warming World. *Journal of Climate*, *33*(2), 443–459. https://doi.org/10.1175/JCLI-D-19-0479.1

Ramirez, C., Nyblade, A., Emry, E. L., Julià, J., Sun, X., Anandakrishnan, S., et al. (2017). Crustal structure of the Transantarctic Mountains, Ellsworth Mountains and Marie Byrd Land, Antarctica: Constraints on shear wave velocities, Poisson's ratios and Moho depths. *Geophysical Journal International*, *211*(3), 1328–1340. https://doi.org/10.1093/gji/ggx333

Ramirez, C., Nyblade, A., Hansen, S. E., Wiens, D. A., Anandakrishnan, S., Aster, R. C., et al. (2016). Crustal and upper-mantle structure beneath ice-covered regions in Antarctica from S-wave receiver functions and implications for heat flow. *Geophysical Journal International*, *204*(3), 1636–1648. https://doi.org/10.1093/gji/ggv542

Randall, D. E., & Mac Niocaill, C. (2004). Cambrian palaeomagnetic data confirm a Natal Embayment location for the Ellsworth—Whitmore Mountains, Antarctica. Gondwana reconstructions. *Geophysical Journal International*, *157*(1), 105–116. https://doi.org/10.1111/j.1365-246X.2004.02192.x

Reading, A. M. (2007). The seismicity of the Antarctic plate. *Geological Society of America Special Paper*, *425*, 285–298. https://doi.org/10.1130/2007.2425(18)

Rignot, E., Mouginot, J., Scheuchl, B., van den Broeke, M., van Wessem, J., & Morlighem, M. (2019). Four decades of Antarctic Ice Sheet mass balance from 1979–2017. *Proceedings of the National Academy of Sciences*, *116*(4), 1095–1103.

Riley, T. R., Flowerdew, M. J., Pankhurst, R. J., Leat, P. T., Millar, I. L., Fanning, C. M., et al. (2017). A revised geochronology of Thurston Island, West Antarctica, and correlations along the proto-Pacific margin of Gondwana. *Antarctic Science*, *29*(1), 47–60. https://doi.org/10.1017/S0954102016000341

Riley, T. R., Jordan, T. A., Leat, P. T., Curtis, M. L., & Millar, I. L. (2020). Magmatism of the Weddell Sea rift system in Antarctica: Implications for the age and mechanism of rifting and early stage Gondwana breakup. *Gondwana Research*, *79*, 185–196. https://doi.org/10.1016/j.gr.2019.09.014

Rivera, A., Uribe, J., Zamora, R., & Oberreuter, J. (2015). Subglacial Lake CECs: Discovery and in situ survey of a privileged research site in West Antarctica. *Geophysical Research Letters*, *42*, 3944–3953. https://doi.org/10.1002/2015GL063390

Rowley, P. D., Thomson, J. W., Smellie, J. L., Laudon, T. S., La Prade, K. E., & LeMasurier, W. E. (1990). Alexander Island, Palmer Land, and Ellsworth Land. In W. E. LeMasurier, & J. W. Thomson (Eds.), Volcanoes of the Antarctic plate and southern oceans, Antarctic Research series (Vol. 48, pp. 296–298). Washington, DC: American Geophysical Union.

Schopf, J. M. (1969). Ellsworth Mountains: Position in West Antarctica due to seafloor spreading. *Science*, *164*, 63–66.

Schutt, D. L., Lowry, A. R., & Buehler, J. S. (2018). Moho temperature and mobility of lower crust in the western United States. *Geology*, *46*(3), 219–222. https://doi.org/10.1130/G39507.1

Seroussi, H., Ivins, E. R., Wiens, D. A., & Bondzio, J. (2017). Influence of a West Antarctic mantle plume on ice sheet basal conditions. *Journal of Geophysical Research: Solid Earth*, *122*, 7127–7155. https://doi.org/10.1002/2017JB014423

Shen, W., Wiens, D. A., Anandakrishnan, A., Aster, R. C., Gerstoft, P., Bromirski, P., et al. (2018). The crust and upper mantle structure of central and West Antarctica from Bayesian inversion of Rayleigh wave and receiver functions. *Journal of Geophysical Research*, *123*. https://doi.org/10.1029/2017JB015346

Shen, W., Wiens, D., Lloyd, A., & Nyblade, A. (2020). A geothermal heat flux map of Antarctica empirically constrained by seismic structure. *Geophysical Research Letters*, *47*. https://doi.org/10.1029/2020GL086955

Shepherd, A., Gilbert, L., Muir, A. S., Konrad, H., McMillan, M., Slater, T., et al. (2019). Trends in Antarctic Ice Sheet elevation and mass. *Geophysical Research Letters*, *46*, 8174–8183. https://doi.org/10.1029/2019GL082182

Siddoway, C. S., & the 10th ISAES editorial team (2008). Tectonics of the West Antarctic rift system: New light on the history and dynamics of distributed intracontinental extension. In A. K. Cooper, P. Barrett, H. Stagg, B. Storey, E. Stump, & W. Wise (Eds.), *Antarctica: A keystone in a changing World* (pp. 91–114). Washington, DC: National Academy of Sciences.

Siegert, M. J., Hindmarsh, R., Corr, H., Smith, A., Woodward, J., King, E. C., et al. (2004). Subglacial Lake Ellsworth: A candidate for in situ exploration in West Antarctica. *Geophysical Research Letters*, *31*(23). https://doi.org/10.1029/2004GL021477

Smith, A. M. (2006). Microearthquakes and subglacial conditions. *Geophysical Research Letters*, *33*. https://doi.org/10.1029/2006GL028207

Snoke, J. A. (2003). FOCMEC: FOCal MEChanism determinations. In W. H. K. Lee, H. Kanamori, P. C. Jennings, & C. Kisslinger (Eds.), *International handbook of earthquake and engineering Seismology*. San Diego, CA: Academic Press.

Steffen, R., Eaton, D. W., & Wu, P. (2012). Moment tensors, state of stress and their relation to post-glacial rebound in northeastern Canada. *Geophysical Journal International*, *189*, 1741–1752. https://doi.org/10.1111/j.1365-246X.2012.05452.x

Stenoien, M. D., & Bentley, C. R. (2000). Pine Island Glacier, Antarctica: A study of the catchment using interferometric synthetic aperture radar measurements and radar altimetry. *Journal of Geophysical Research*, *105*(B9), 21761–21770. https://doi.org/10.1029/2000JB900151

Sugden, D. E., Hein, A. S., Woodward, J., Marrero, S. M., Rodés, A., Dunning, S. A., et al. (2017). The million-year evolution of the glacial trimline in the southernmost Ellsworth Mountains, Antarctica. *Earth and Planet Science Lett*, *469*, 42–52. https://doi.org/10.1016/j.epsl.2017.04.006

Tesauro, M., Kaban, M. K., & Mooney, W. D. (2015). Variations of the lithospheric strength and elastic thickness in North America. *Geochemistry, Geophysics, Geosystems*, *16*, 2197–2200. https://doi.org/10.1002/2015GC005937

Weaver, S. D., Storey, B. C., Pankhurst, R. J., Mukasa, S. B., DiVenere, V. J., & Bradshaw, J. D. (1994). Antarctica–New Zealand rifting and Marie Byrd Land lithospheric magmatism linked to ridge subduction and mantle plume activity. *Geology*, *22*(9), 811–814. https://doi.org/10.1130/0091-7613(1994)022<0811:ANZRAM>2.3.CO;2

West, M., Larsen, C. F., Truffer, M., O'Neel, S., & LeBlanc, L. (2010). Glacier microseismicity. *Geology*, *38*, 319–322. https://doi.org/10.1130/G30606.1

White-Gaynor, A. L., Nyblade, A. A., Aster, R. C., Wiens, D. A., Bromirski, P. D., Gerstoft, P., et al. (2019). Heterogeneous upper mantle structure beneath the Ross Sea Embayment and Marie Byrd Land, West Antarctica, revealed by P- wave tomography. *Earth and Planetary Science Letters*, *513*, 40–50. https://doi.org/10.1016/j.epsl.2019.02.013

Whitehouse, P. L., Gomez, N., King, M. A., & Wiens, D. A. (2019). Solid Earth change and the evolution of the Antarctic Ice Sheet. *Nature Communications*, *10*(503). https://doi.org/10.1038/s41467-018-08068-y

Winberry, J. P., & Anandakrishnan, S. (2003). Seismicity and neotectonics of West Antarctica. *Geophysical Research Letters*, *30*(18). https://doi.org/10.1029/2003gl018001

Winberry, J. P., Huerta, A. D., Anandakrishnan, S., Aster, R. C., Nyblade, A. A., & Wiens, D. A. (2020). Glacial earthquakes and precursory seismicity associated with Thwaites Glacier calving. *Geophysical Research Letters*, *47*. https://doi.org/10.1029/2019GL086178

Zundel, M., Spiegel, C., Mehling, A., Lisker, F., Hillenbrand, C. D., Monien, P., et al. (2019). Thurston Island (West Antarctica) between Gondwana subduction and continental separation: A multistage evolution revealed by apatite thermochronology. *Tectonics*, *38*, 878–897. https://doi.org/10.1029/2018TC005150

References From the Supporting Information

Morlighem, M., Rignot, E., Binder, T., Blankenship, D., Drews, R., Eagles, G., et al. (2020). Deep glacial troughs and stabilizing ridges unveiled beneath the margins of the Antarctic ice sheet. *Nature Geoscience*, *13*, 132–137. https://doi.org/10.1038/s41561-019-0510-8